

How clustered protocadherin binding specificity is tuned for neuronal self-/nonself-recognition

Kerry Marie Goodman^{1†}, Phinikoula S Katsamba^{1†}, Rotem Rubinstein^{2,3}, Göran Ahlsén¹, Fabiana Bahna¹, Seetha Mannepli¹, Hanbin Dan⁴, Rosemary V Sampogna⁴, Lawrence Shapiro^{1,5*}, Barry Honig^{1,4,5,6*}

¹Zuckerman Mind, Brain and Behavior Institute, Columbia University, New York, United States; ²School of Neurobiology, Biochemistry and Biophysics, Tel Aviv University, Tel Aviv, Israel; ³Sagol School of Neuroscience, Tel Aviv University, Tel Aviv, Israel; ⁴Department of Medicine, Division of Nephrology, Columbia University, New York, United States; ⁵Department of Biochemistry and Molecular Biophysics, Columbia University, New York, United States; ⁶Department of Systems Biology, Columbia University, New York, United States

Abstract The stochastic expression of fewer than 60 clustered protocadherin (cPcdh) isoforms provides diverse identities to individual vertebrate neurons and a molecular basis for self-/nonself-discrimination. cPcdhs form chains mediated by alternating *cis* and *trans* interactions between apposed membranes, which has been suggested to signal self-recognition. Such a mechanism requires that cPcdh *cis* dimers form promiscuously to generate diverse recognition units, and that *trans* interactions have precise specificity so that isoform mismatches terminate chain growth. However, the extent to which cPcdh interactions fulfill these requirements has not been definitively demonstrated. Here, we report biophysical experiments showing that cPcdh *cis* interactions are promiscuous, but with preferences favoring formation of heterologous *cis* dimers. *Trans* homophilic interactions are remarkably precise, with no evidence for heterophilic interactions between different isoforms. A new C-type cPcdh crystal structure and mutagenesis data help to explain these observations. Overall, the interaction characteristics we report for cPcdhs help explain their function in neuronal self-/nonself-discrimination.

***For correspondence:**
lss8@columbia.edu (LS);
bh6@cumc.columbia.edu (BH)

[†]These authors contributed equally to this work

Competing interest: The authors declare that no competing interests exist.

Funding: See page 22

Received: 22 July 2021

Preprinted: 23 July 2021

Accepted: 26 January 2022

Published: 07 March 2022

Reviewing Editor: Kang Shen, Howard Hughes Medical Institute, Stanford University, United States

© Copyright Goodman et al. This article is distributed under the terms of the [Creative Commons Attribution License](https://creativecommons.org/licenses/by/4.0/), which permits unrestricted use and redistribution provided that the original author and source are credited.

Editor's evaluation

The direct investigation of homotypic and heterotypic preference between *cis* and *trans* interactions among the protocadherin isoforms is an important step to understand the mechanisms of self avoidance. We are particularly excited about the discovery that the discovery that showed *cis* interactions are promiscuous, but with preferences favoring formation of heterologous *cis* dimers. *Trans*-homophilic interactions are remarkably precise, with no evidence for heterophilic interactions between different isoforms.

Introduction

Clustered protocadherins (cPcdhs) are a large family of cadherin-like proteins named for the clustered arrangement of their genes in vertebrate genomes (*Wu and Maniatis, 1999; Wu et al., 2001*). cPcdhs

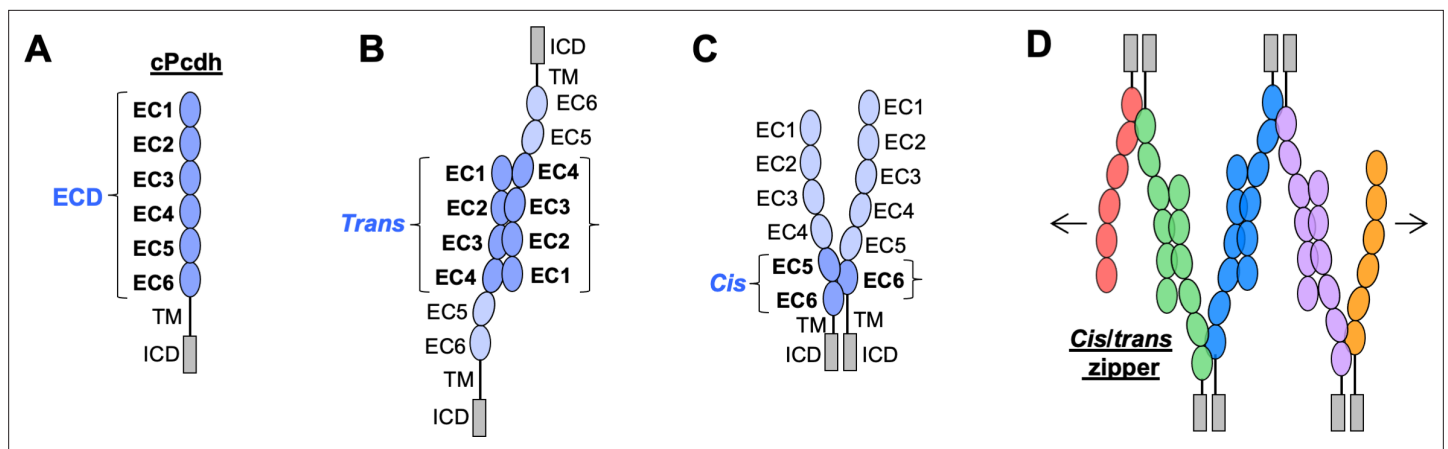


Figure 1. Clustered protocadherin (cPcdh) domain organization and extracellular interactions. **(A)** Schematic depicting the domain organization of cPcdhs. EC, extracellular cadherin domain; TM, transmembrane domain; ECD, ectodomain; ICD, intracellular domain. **(B)** Schematic of two cPcdhs interacting via the EC1–4 *trans* interface. **(C)** Schematic of two cPcdhs interacting via the EC5–6/EC6 *cis* interface. **(D)** Schematic depiction of the *cis/trans* cPcdh zipper comprising multiple cPcdh isoforms (various colors) engaged in homophilic *trans* interactions and promiscuous *cis* interactions as required for the proposed ‘isoform-mismatch chain-termination model’ of cPcdh-mediated neuronal self-recognition and self-avoidance.

play roles in many facets of neural development (Peek *et al.*, 2017), including circuit development, most notably neurite self-avoidance in vertebrates (Kostadinov and Sanes, 2015; Lefebvre *et al.*, 2012; Mountoufaris *et al.*, 2017), and tiling (Chen *et al.*, 2017). In self-avoidance, neurites from the same neuron (sister neurites) actively avoid one another, whereas neurons from different neurons can freely interact. Tiling is similar to self-avoidance, but in tiling all neurons acquire the same identity, so that there is uniform repulsion among self- and nonself-neurites (Chen *et al.*, 2017). Self-avoidance among sister neurites leads to the characteristic arbor structures of dendritic trees, and prevents the formation of self-synapses (Kostadinov and Sanes, 2015; Lefebvre *et al.*, 2012).

The molecular mechanisms through which neurons discriminate self from nonself, differ between vertebrate and most invertebrate animals. For arthropod invertebrates such as *Drosophila melanogaster*, self-avoidance is mediated by immunoglobulin superfamily Dscam1 cell surface proteins. The stochastic alternative splicing of *Dscam1* pre-mRNAs can, in principle, generate 19,008 distinct extracellular isoforms; the vast majority of which, based on ELISA-based binding assays, mediate homophilic recognition (Miura *et al.*, 2013; Schmucker *et al.*, 2000; Wojtowicz *et al.*, 2004; Wojtowicz *et al.*, 2007). Each *Drosophila* neuron expresses a repertoire estimated at 10–50 isoforms and the large number of Dscam1 isoforms ensures a low probability that any two contacting neurons will have an identical or even a similar isoform repertoire thus minimizing the chance of inappropriate avoidance between nonself-neurons (Hattori *et al.*, 2009).

In mammalian nervous systems, cPcdh isoform expression is controlled by the unique organization of three tandem gene clusters, *Pcdhα*, *Pcdhβ*, and *Pcdhγ* (Wu and Maniatis, 1999), with each cluster containing multiple variable exons, which encode full cPcdh ectodomain regions with six extracellular cadherin (EC) domains, a single transmembrane region, and a short cytoplasmic extension (Figure 1A). The *Pcdhα* and *Pcdhγ* gene clusters also contain three ‘constant’ exons that encode cluster-specific intracellular domains. The last two variable exons in the *Pcdhα* gene cluster and the last three variable exons of the *Pcdhγ* gene cluster diverge in sequence from other cPcdh isoforms and are referred to as ‘C-type’ cPcdhs (Wu and Maniatis, 1999; Wu *et al.*, 2001). Sequence differences further subdivide *Pcdhγ* genes into two subfamilies – *PcdhγA* and *PcdhγB* (Wu and Maniatis, 1999). The full mouse cPcdh complement is comprised of 53 non-C-type cPcdhs, commonly known as alternate cPcdhs (α1–12, β1–22, γA1–12, and γB1–7), whose expression choices vary stochastically between cells through alternate promoter choice (Canzio and Maniatis, 2019) and 5 C-type cPcdhs (αC1, αC2, γC3, γC4, and γC5), which are constitutively expressed. cPcdh expression, either stochastic or constitutive, varies between cell types: for example, olfactory sensory neurons express ~5–10 cPcdhs stochastically; Purkinje neurons express ~10 alternate cPcdhs stochastically and all five C-types constitutively (Esumi *et al.*, 2005; Kaneko *et al.*, 2006); and serotonergic neurons express just αC2 constitutively (Canzio and Maniatis, 2019; Chen *et al.*, 2017). While the cPcdh and Dscam1

systems bear striking similarities, the relatively small number of cPcdh isoforms – fewer than 60 – has presented a significant challenge to generation of sufficient diversity to provide mammalian neurons with functionally unique identities.

Solution biophysics and functional mutagenesis studies have shown that cPcdhs interact in *trans* through antiparallel interactions between their EC1–4 regions (Rubinstein et al., 2015), and crystal structures of alternate α , β , and γ cPcdh *trans* homodimers have revealed interfaces involving EC1 interacting with EC4 and EC2 with EC3 (Figure 1B; Goodman et al., 2016c; Goodman et al., 2016a; Nicoludis et al., 2016; Rubinstein et al., 2015; Thu et al., 2014). cPcdhs also form *cis* dimers through their membrane-proximal EC5–6 regions, and are presented on cell surfaces as *cis* dimers (Goodman et al., 2017; Rubinstein et al., 2015; Thu et al., 2014). Crystal structures of *cis*-interacting protocadherin ectodomains (Brasch et al., 2019; Goodman et al., 2017) have revealed an asymmetrical interaction mode, where one molecule interacts through elements of EC5 and EC6, and the other interacts exclusively through EC6 (Figure 1C). To date, structural studies of C-type cPcdh interactions have not been available. Here, we extend our molecular understanding of cPcdhs to C-type isoforms as well, with the goal of understanding the evolutionary design of the entire family.

In order to explain how about 60 cPcdh isoforms can provide a comparable or even greater level of neuronal diversity as 19,000 Dscam isoforms, Rubinstein et al., 2015 proposed that cPcdhs located on apposed membrane surfaces would form an extended zipper-like lattice through alternating *cis* and *trans* interactions (Figure 1D). In self-interactions – between two membranes with identical cPcdh repertoires – these chains would grow to form large structures, limited mainly by the number of molecules (Brasch et al., 2019; Rubinstein et al., 2015). However, in nonself-interactions – between two membranes with differing cPcdh repertoires – such large linear assemblies would not form since even a single mismatch between expressed isoforms would terminate chain assembly (Brasch et al., 2019; Rubinstein et al., 2017; Rubinstein et al., 2015). This ‘isoform-mismatch chain-termination model’ for the ‘barcoding’ of vertebrate neurons envisions the assembly of long cPcdh chains between sites of neurite–neurite contact to represent the signature of ‘self’, which is then translated by downstream signaling that leads to self-avoidance (Fan et al., 2018). X-ray crystallographic studies and cryo-electron tomography studies of the full-length cPcdh ectodomains bound between the surfaces of adherent liposomes revealed the existence of linear zippers thus providing strong evidence supporting the validity of the model (Brasch et al., 2019). However, crucial questions remain unanswered. Here, a number of them are addressed.

1. For the proposed mechanism to successfully explain neuronal barcoding, *cis* interactions must be promiscuous to generate diverse repertoires of *cis*-dimeric biantennary ‘interaction units’, while *trans* interactions must be highly specific so that mismatched isoforms do not inappropriately enable growth of the chain through heterophilic interactions. While cell aggregation assays have suggested *trans* homophilic specificity, these assays only reflect a *competition* between different cell populations and thus do not inform as to the strength of heterophilic interactions. Moreover, the results of cell aggregation assays depend critically on the *relative* strengths of homophilic and heterophilic interactions and thus do not inform as to actual binding affinities (Honig and Shapiro, 2020). It is thus necessary to establish the extent to which heterophilic *trans* interactions are truly disallowed.
2. The assumption that *cis* interactions are promiscuous is based in large part on the fact that α -cPcdhs and γ C4 cannot reach the cell surface without binding in *cis* to another ‘carrier’ isoform (Bonn et al., 2007; Goodman et al., 2016a; Murata et al., 2004; Schreiner and Weiner, 2010; Thu et al., 2014). As is the case for *trans* interactions, the strength of *cis* interactions has only been probed quantitatively in a small number of cases so that the term ‘promiscuous’ is qualitative at best. In fact, as compared to γ B and β cPcdh isoforms, most γ A-Pcdhs do not form measurable *cis* homodimers in solution (Goodman et al., 2016a; Figure 4—source data 1). Nevertheless, all γ A-Pcdhs are still able to reach the cell surface when expressed alone (Thu et al., 2014). This observation can be understood if the *cis* dimerization affinity of γ A-Pcdhs is large enough to enable them to dimerize in the 2D membrane environment (Goodman et al., 2016a; Wu et al., 2013). Nevertheless, their weak dimerization affinities suggest, more generally, that cPcdhs may exhibit a range of *cis* dimerization affinities. We establish below that a wide range of affinities does in fact exist and, strikingly, most homophilic *cis* interactions are weaker than their heterophilic counterparts. We consider the functional implications of this novel observation in the discussion.

3. Structures have not yet been determined for complete C-type cPcdh ectodomains. Yet these isoforms play unique functional roles, some of which have no apparent connection to isoform diversity. For example, a single C-type isoform is sufficient for tiling which can be simply understood in terms of the formation of zippers containing identical homodimers so that all interacting neurons will avoid one another (Chen et al., 2017). Moreover, Garrett et al. discovered that neuronal survival and postnatal viability are controlled solely by γ C4 suggesting a function that is unique to this isoform (although it presumably requires β and/or other γ carriers to reach the cell surface) (Garrett et al., 2019). Additionally, a recent paper by Iqbal et al. has shown that genetic γ C4 variants cause a neurodevelopmental disorder which is potentially linked to γ C4's role in programmed cell death of neuronal cells (Iqbal et al., 2021). Below we report extensive biophysical interaction studies of C-type isoform ectodomains and report the first crystal structure of a *trans* dimer formed by γ C4. Our findings reveal that the specialized functions of C-type cPcdhs probably do not involve unique structural or biophysical properties of their ectodomains.

Overall, in accordance with the requirements of the isoform-mismatch chain-termination model, we find that *trans* homophilic interactions are remarkably precise, with no evidence for heterophilic interactions between different cPcdh isoforms. In contrast cPcdh *cis* interactions are largely promiscuous but with relatively weak intrasubfamily and, especially, homophilic interactions. Possible implications of this somewhat surprising finding are considered in the discussion. Our study reveals how the extraordinary demands posed by the need to assign each neuron with a unique identity are met by an unprecedented level of protein–protein interaction specificity.

Results

cPcdh *trans* interactions are strictly homophilic

We generated biotinylated ectodomain fragments containing the *trans*-interacting EC1–4 regions (Nicoludis et al., 2015; Rubinstein et al., 2015) of six representative α , β , γ A, and γ B mouse cPcdh isoforms – α 7, β 6, β 8, γ A8, γ A9, and γ B2 – which include the most closely related isoforms by sequence identity from the β and γ A subfamilies (β 6/8 and γ A8/9) (Rubinstein et al., 2015). These molecules were coupled over independent NeutrAvidin-immobilized flow cells and *trans*-interacting ectodomain fragments of multiple members of each mouse cPcdh subfamily, including the C-types (α 4, α 7, α 12, β 6, β 8, γ A4, γ A8, γ A9, γ B2, γ B4, γ B5, α C2, γ C3, γ C4, and γ C5), were then flowed over the six cPcdh surfaces to assess their binding. The surface plasmon resonance (SPR)-binding profiles reveal strictly homophilic binding (Figure 2A). All ectodomain fragments used in these SPR experiments were confirmed to form homodimers in solution by sedimentation equilibrium analytical ultracentrifugation (AUC) (Figure 2—source data 1), validating that these proteins are well behaved and active. Remarkably, no heterophilic binding was observed for any of the analytes over any of the six surfaces (Figure 2A). Even β 6/8 and γ A8/9 that have 92% and 82% sequence identities, respectively, in their *trans*-binding EC1–4 regions exhibit no heterophilic binding. We estimate that, for heterophilic *trans* dimers, the lower limit for the dissociation constant (K_D) would be \sim 200 μ M. Mutations designed to disrupt α 7, β 6, and γ A8 *trans* interaction inhibited homophilic binding, demonstrating that the observed binding occurs via the *trans* interface (Figure 2—figure supplement 1A; Goodman et al., 2016a; Goodman et al., 2016c; Rubinstein et al., 2015). This behavior is unlike that of other adhesion receptor families where, whether they display homophilic or heterophilic preferences, the signal is never as binary as the one shown in Figure 2 (Honig and Shapiro, 2020).

Much of the original evidence as to homophilic specificity was based on cell aggregation assays (Rubinstein et al., 2015; Schreiner and Weiner, 2010; Thu et al., 2014) and it is of interest to compare the results obtained from these assays to those obtained from SPR. We do this in the context of examining the heterophilic binding specificity between β 6_{1–4} and β 8_{1–4}*trans* fragments that share 92% sequence identity and differ at only five residues (Figure 2—figure supplement 2A), within their respective binding interfaces (Goodman et al., 2016c). Each of these residues was mutated individually and in combination. Figure 2—figure supplement 2B, C displays SPR profiles and cell aggregation images, respectively, for wild-type β 6 and β 8 and for the various mutations. We first note that changing all five residues in β 6 to those of β 8 generates a mutant protein with essentially wild-type β 8 properties; it binds strongly to β 8 but not to β 6 as seen in SPR and also forms mixed aggregates with β 8 but not β 6. In contrast, most of the single residue mutants retain β 6-like properties in both assays whereas double and triple mutants exhibit intermediate behavior between β 6 and β 8. These

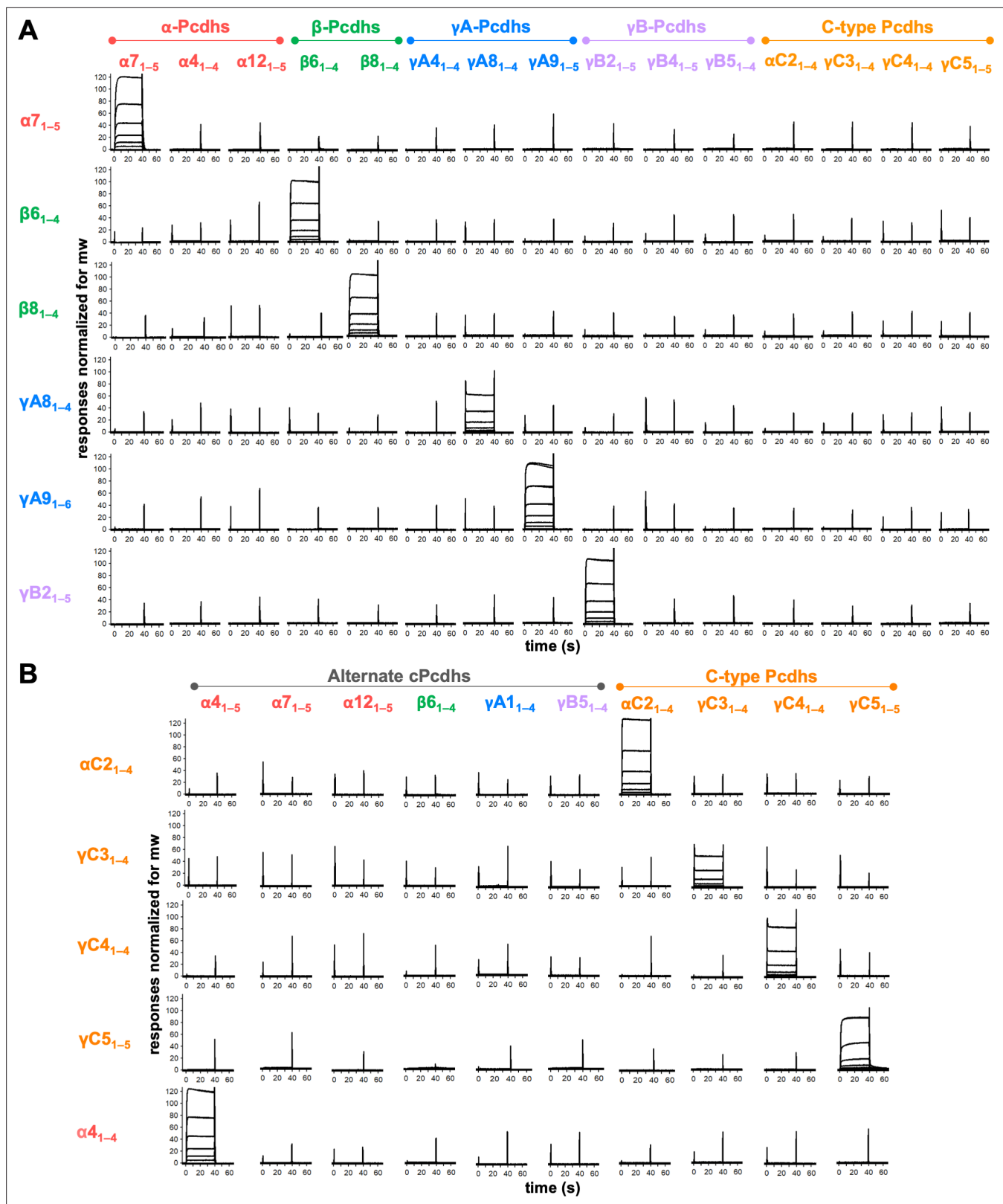


Figure 2. Clustered protocadherins (cPcdhs) show strict homophilic specificity in their *trans* interactions. **(A)** Surface plasmon resonance (SPR) binding profiles of cPcdh *trans* fragment analytes from all cPcdh subfamilies (denoted in the top row) flowed over six surfaces coated with alternate cPcdh *trans* fragments (rows). Responses over all surfaces are drawn on the same scale and normalized for molecular weight (mw). **(B)** SPR binding profiles of cPcdh

Figure 2 continued on next page

Figure 2 continued

trans fragment analytes from all cPcdh subfamilies (shown in columns) flowed over individual surfaces coated with C-type and $\alpha 4$ cPcdh *trans* fragments (rows). Responses over all surfaces are drawn on the same scale and normalized for molecular weight.

The online version of this article includes the following source data and figure supplement(s) for figure 2:

Source data 1. Sedimentation equilibrium analytical ultracentrifugation data for *trans* SPR reagents.

Figure supplement 1. *Trans* interface mutants demonstrate homophilic interactions observed in surface plasmon resonance (SPR) are mediated by the *trans* dimer interface.

Figure supplement 2. Mutagenesis experiments reveal role in *trans* specificity for the five interfacial residue differences between close pair $\beta 6_{1-4}$ and $\beta 8_{1-4}$.

results demonstrate that despite the 92% sequence identity between $\beta 6$ and $\beta 8$, their highly specific homophilic properties can be attributed to five interfacial residues. Moreover, the cell aggregation assays are consistent with the heterophilic binding traces measured by SPR; cells expressing mutants that generate strong SPR signals with either wild-type $\beta 6$ or $\beta 8$ also form mixed aggregates with cells expressing the same wild-type protein.

Of note, *trans*-interacting fragments of all four C-type cPcdhs tested showed no binding over the alternate cPcdh SPR surfaces (**Figure 2A**). To test whether C-type cPcdhs also show strict homophilic specificity with respect to each other we coupled biotinylated *trans*-interacting fragments of $\alpha C2$, $\gamma C3$, $\gamma C4$, and $\gamma C5$ to SPR chips and passed the same four fragments alongside alternate cPcdh *trans* fragments over these four surfaces. Only homophilic binding was observed, with each of the four C-type fragments binding to its cognate partner and no other isoform (**Figure 2B**). Disrupting the $\gamma C5$ *trans* interaction with the S116R mutation (**Rubinstein et al., 2015**), inhibited binding to the $\gamma C5$ surface, demonstrating that the observed binding occurs via the *trans* interface (**Figure 2—figure supplement 1B**).

In contrast to the other C-type isoforms, $\alpha C1$ does not mediate cell–cell interactions in cell aggregation assays even when coexpressed with cPcdhs that facilitate cell-surface delivery of $\gamma C4$ (**Thu et al., 2014**). Although we have been able to produce an $\alpha C1$ EC1–4 fragment the recombinant molecule forms disulfide-linked multimers which are likely nonnative, precluding confident examination of $\alpha C1$'s potential *trans* interactions. Notably, the sequence of mouse $\alpha C1$ reveals the EC3:EC4 linker does not contain the full complement of calcium-coordinating residues, which may impact the structure and binding properties of this protein (**Thu et al., 2014**).

Since all the cPcdh *trans* fragment molecules used in these SPR experiments homodimerize our SPR data cannot be used to determine accurate binding affinities (**Rich and Myszka, 2007**). We therefore used AUC to measure the *trans* homodimer K_{DS} (**Figure 2—source data 1**) revealing a >200-fold range of binding affinities, from 2.9 μM ($\alpha 7_{1-5}$) to >500 μM ($\gamma C4_{1-4}$). Regardless of their *trans*-binding affinity, all cPcdhs (except $\alpha C1$) have previously been shown to effectively mediate cell–cell interactions in cell aggregation assays (**Schreiner and Weiner, 2010; Thu et al., 2014**).

Crystal structure of C-type cPcdh $\gamma C4$ reveals EC1–4-mediated head-to-tail *trans* dimer interaction

The biophysical properties of C-type cPcdhs pose a number of interesting questions: Despite their more divergent sequences compared with alternate cPcdhs, AUC data have confirmed that C-type cPcdhs $\alpha C2$, $\gamma C3$, and $\gamma C5$ form *trans* dimers using their EC1–4 domains (**Goodman et al., 2016a; Rubinstein et al., 2015**). However, $\gamma C4_{1-4}$ behaved as a very weak dimer in AUC ($K_D > 500 \mu M$; **Figure 2—source data 1**), nevertheless full-length $\gamma C4$ can mediate cell aggregation when delivered to the cell surface by coexpression with a 'carrier' cPcdh (**Thu et al., 2014**). In addition, C-type isoforms have unique expression profile and function compared to alternate cPcdhs (**Canzio and Maniatis, 2019; Mountoufaris et al., 2018**). However, there are no published crystal structures of C-type cPcdh *trans* dimers. We therefore sought to crystallize a mouse C-type cPcdh engaged in a *trans* interaction and obtained two distinct crystal forms of $\gamma C4_{EC1-4}$, one at 2.4 Å resolution (crystallized at pH 7.5) and the other with anisotropic diffraction at 4.6/3.9/3.5 Å resolution (**Figure 3A, Figure 3—figure supplement 1A, B, Figure 3—source data 1**) (crystallized at pH 6.0). Both crystal structures revealed an EC1–4-mediated head-to-tail *trans* dimer: The 4.6/3.9/3.5 Å crystal structure appears to have a fully intact *trans* interface with a total buried surface area of 3800 Å², which is a similar size to other cPcdh *trans*

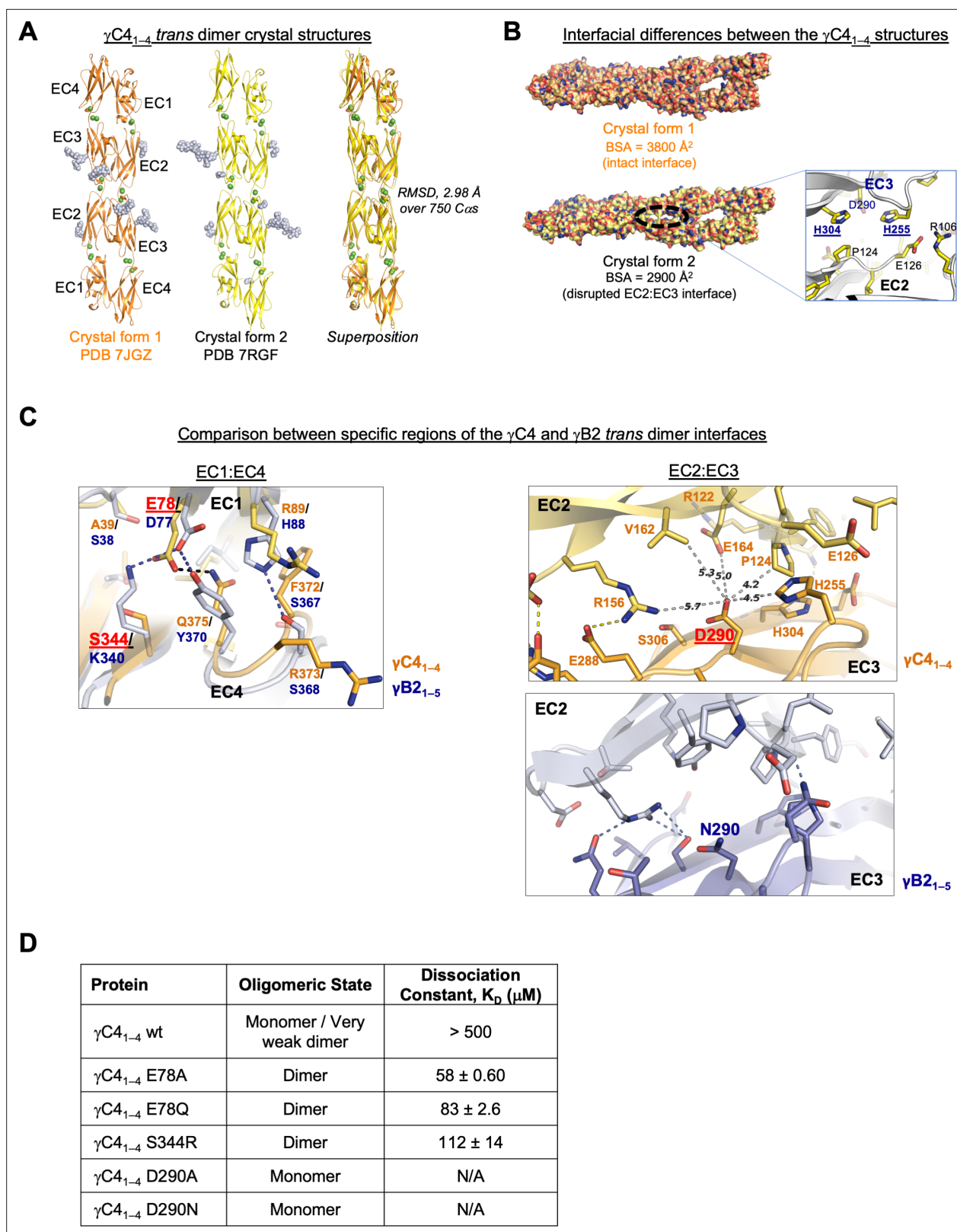


Figure 3. C-type clustered protocadherin (cPcdh) $\gamma C4$ adopts an EC1–4-mediated head-to-tail *trans* dimer like alternate cPcdhs with a comparatively weak dimer affinity. (A) Ribbon diagrams of the $\gamma C4_{EC1-4}$ *trans* dimer crystal structures obtained from two different crystal forms. Bound calcium ions are shown as green spheres and glycans are shown in pale blue spheres. (B) The two crystal structures have a markedly different *trans* interface buried surface area (BSA). Left, surface views of the two *trans* dimer crystal structures highlight the difference, with a gap apparent in the EC2:EC3 region of Figure 3 continued on next page

Figure 3 continued

the interface in crystal form two that is absent from crystal form 1. Surfaces are colored by atom type with the carbons colored orange for crystal form one and yellow for crystal form 2. *Right*, close-up view of the gap region in the crystal form two dimer with the side chains depicted as sticks. The intact crystal form 1 γ C4 dimer is similar overall to those of the published intact alternate α , β , γ A, and γ B cPcdhs and the published δ 2 nonclustered (nc) Pcdh *trans* dimers (root mean square deviation [RMSD] over aligned C α s 2.4–4.5 Å; **Figure 3—source data 2**). The published crystal structures of γ A1, γ A8, and γ B3 also show partially disrupted *trans* interfaces though in differing regions of the interface (**Goodman et al., 2016a, Nicoludis et al., 2016**). **(C)** Comparison between the (i) EC1:EC4 and (ii) EC2:EC3 regions of the γ C4 (orange) and γ B2 (blue, PDB 5T9T) *trans* dimer interfaces. Potential hydrogen bonds are depicted as dashed black/yellow (γ C4) or blue (γ B2) lines. (i) Structural alignment of the EC1:EC4 portion of the γ C4 and γ B2 *trans* dimers highlights a possible destabilizing role for γ C4 residue E78 since unlike its counterpart in γ B2 (D77), it is not juxtaposed with a basic residue. (ii) Similarly, an additional negatively charged residue (D290) which occupies a central position in the γ C4 EC2:EC3 interface may also contribute to γ C4's comparatively weak *trans* dimer interaction. Distances between the D290 side chain and its nearest contacts are shown as dashed gray lines with distances given in Angstroms. **(D)** Sedimentation equilibrium analytical ultracentrifugation (AUC) experiments were conducted on γ C4 EC1–4 wild-type (wt) and interface mutants to assess whether E78 and D290 negatively impact *trans* dimerization. Table details the oligomeric state and dissociation constants for each protein tested.

The online version of this article includes the following source data and figure supplement(s) for figure 3:

Source data 1. X-ray crystallography data collection and refinement statistics.

Source data 2. Overall structural similarity between cPcdh γ C4, alternate cPcdhs, and non-clustered Pcdhs *trans* dimer structures.

Figure supplement 1. γ C4 *trans* dimer crystal structures and *trans* interface analysis.

dimer interfaces (**Goodman et al., 2016a; Goodman et al., 2016c; Nicoludis et al., 2016; Figure 3B, Figure 3—figure supplement 1B**). However, the 2.4 Å structure had an apparently partially disrupted EC2:EC3 interface resulting in a total buried surface area of just 2900 Å² (**Figure 3B**). The difference between the two structures may be due to differences in the pH of the crystallization and its effect on the ionization state of the three histidines present in the EC2:EC3 interface (**Figure 3B**). The differences could also reflect distinct states of a dynamic interaction, as has previously been observed crystallographically (**Nicoludis et al., 2016; Goodman et al., 2016a**) and explored computationally for other cPcdh *trans* interactions (**Nicoludis et al., 2019**).

Despite the γ C4 *trans* dimer sharing structural similarity and the interface having similar buried surface area as alternate α , β , γ A, and γ B cPcdhs and δ 2 nonclustered Pcdhs (**Figure 3—source data 2; Cooper et al., 2016; Goodman et al., 2016a; Goodman et al., 2016c; Harrison et al., 2020; Hudson et al., 2021; Nicoludis et al., 2016**), its binding affinity is very weak. The two most structurally similar molecules to γ C4 over their *trans*-interacting domains are cPcdh γ B2 and nonclustered Pcdh19. γ B2 and Pcdh19 have *trans* dimer K_{DS} of 21.8 and 0.48 μ M, respectively (**Harrison et al., 2020**), while that of γ C4 is >500 μ M. Comparison between the γ B2 and γ C4 dimer interfaces highlighted two buried charges in the γ C4 *trans* interface, E78 and D290, which could potentially contribute to the low interaction affinity (**Figure 3C**). To test this, we mutated these two residues to neutral amino acids and used AUC to determine whether the binding affinity increased: The two D290 mutations we tested, D290A and D290N, had no measurable impact on binding; but mutating E78 significantly increased the binding affinity with γ C4_{EC1–4} E78A showing a K_D of 58 μ M and γ C4_{EC1–4} E78Q, 83 μ M (**Figure 3D, Figure 3—figure supplement 1C**). The equivalent residue to E78 in γ B2 is also charged (D77) and forms a salt bridge with K340 in the γ B2 dimer (**Figure 3C**). To assess whether generating a similar salt bridge in γ C4 would compensate for the negative impact of E78 on dimer affinity we generated an S344R mutant. Similar to the E78 mutants, γ C4_{EC1–4} S344R also had a stronger binding affinity than wild-type with a K_D of 112 μ M (**Figure 3D, Figure 3—figure supplement 1C**). It appears then that E78 plays an important role in weakening cPcdh γ C4's *trans* interaction although the functional reasons for γ C4's weak *trans* interaction are unclear.

cPcdh *cis* interactions are promiscuous with a range of interaction strengths

To systematically investigate cPcdh *cis* interactions, we coupled *cis*-interacting fragments of mouse β 9, γ A4, γ A9, γ B2, α C2, γ C3, and γ C5 to SPR chip surfaces. *Cis*-interacting fragments of three members from each of the β , γ A, and γ B subfamilies (β 1, β 6, β 9, γ A3, γ A4, γ A9, γ B2, γ B5, and γ B7) alongside α C2, γ C3, and γ C5 fragments were flowed over the seven surfaces to detect their heterophilic binding (**Figure 4A**). Alternate α -cPcdhs, and the C-types α C1 and γ C4 were not included in this study since EC6-containing fragments of these molecules cannot be expressed, although an α 7_{EC1–9/}

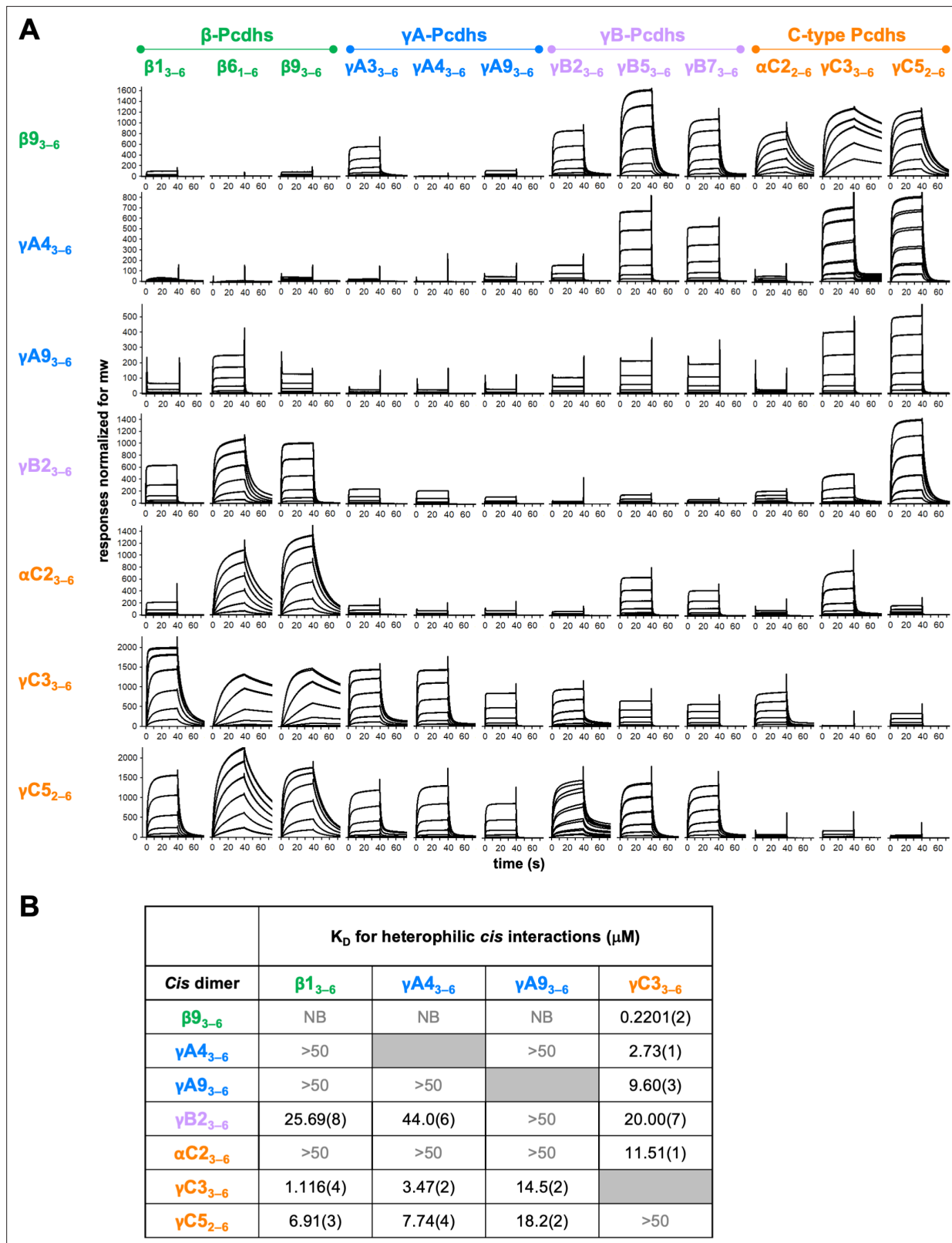


Figure 4. Clustered protocadherin (cPcdh) *cis* interactions are promiscuous with a preference for interfamily heterodimers. **(A)** Surface plasmon resonance (SPR)-binding profiles of cPcdh *cis* fragment analytes from all cPcdh subfamilies except alphas (shown in columns) flowed over individual surfaces coated with cPcdh *cis* fragments. Binding profiles for each surface are individually scaled and responses are normalized for molecular weight. **(B)** Table of dissociation constants calculated from the SPR data for the four monomeric analytes. The number in brackets represents the error of the fit

Figure 4 continued on next page

Figure 4 continued

based on analysis of duplicate responses. Binding signals were not detected for interactions labeled NB (no binding) while >50 represents interactions with K_D s > 50 μ M, where an accurate K_D cannot be determined.

The online version of this article includes the following source data and figure supplement(s) for figure 4:

Source data 1. Sedimentation equilibrium analytical ultracentrifugation data for cis SPR reagents.

Figure supplement 1. Calculation of cis interaction dissociation constants and the impact of an α -Pcdh EC5 on family-wide cis interactions.

Figure supplement 2. Range of clustered protocadherin (cPcdh) cis and trans dissociation constants, K_D s.

Figure supplement 3. Amino acid sequence alignment reveals conservation of cis interfacial residues within the alternate clustered protocadherin (cPcdh) subfamilies.

γ C3_{EC6} chimera was included among the analytes to assess the role of α 7 EC5 (**Figure 4—figure supplement 1C**). Each of the analytes was also analyzed by AUC to determine their homophilic cis-interaction behavior (**Figure 4—source data 1**): Four analytes, β 1_{3-6r}, γ A4_{3-6r}, γ A9_{3-6r}, and γ C3_{3-6r}, are monomeric in solution as measured by AUC, therefore their SPR binding profiles could be analyzed to determine their heterophilic binding affinities (**Figure 4B**, **Figure 4—figure supplement 1A, B**). For the remaining analytes, due to the added complexity of their homophilic cis interactions in solution competing with their binding to the immobilized molecules, the SPR responses could not be analyzed to determine accurate K_D s (**Rich and Myszka, 2007**).

The data clearly demonstrate a wide range of cis dimerization affinities with strong heterophilic binding signals (500–2000 RU), with much weaker homophilic binding responses typically between 100 and 140 RU. The strongest heterophilic cis interactions are in the submicromolar range; for example, γ C3/ β 9 can heterophilically cis-dimerize with a K_D of 0.22 μ M, while β 9_{3-6r}, γ B2_{3-6r}, α C2_{2-6r}, and γ C5₂₋₆ homodimerize with AUC-determined K_D s of 9–80 μ M. In addition to uniformly weak homophilic interactions, within-subfamily cis interactions were consistently among the weakest observed although a number of intersubfamily interactions were also relatively weak (**Figure 4A**). For example, for the β 9 surface comparatively weak binding was observed for all tested β and γ A isoforms except γ A3, with the monomeric β 1, γ A4, and γ A9 producing low responses that could not be fit to a binding isotherm to calculate accurate K_D s (**Figure 4B**, **Figure 4—figure supplement 1B**). In contrast, robust binding to the β 9 surface was observed for all γ B and C-type isoforms. These data are consistent with the binding responses when β 9 was used as an analyte over the other six surfaces, with weak to no binding observed over the γ A4 and γ A9 surfaces and robust responses over the γ B2, α C2, γ C3, and γ C5 surfaces (**Figure 4A**). The γ A4 and γ A9 surfaces showed a similar pattern of binding behaviors, with weak to no binding observed for the γ A and α C2 analytes, and robust binding for the γ C-cPcdhs with K_D s for γ C3₃₋₆ of 2.73 and 9.60 μ M, respectively, over each surface (**Figure 4**, **Figure 4—figure supplement 1B**).

Overall, these SPR data show that cPcdh cis binding is generally promiscuous, with measurable cis interactions observed for 86% of pairs tested (using a 40 RU threshold). However, the wide range of binding responses and homo- and heterodimeric K_D s that span 0.2201 μ M to no measurable interaction in solution suggests certain cis dimers will form preferentially to others. For the heterophilic binding pairs for which K_D s could be determined (**Figure 4B**, **Figure 4—figure supplement 1**, **Figure 4—figure supplement 2**), the alternate cPcdhs in particular, form markedly stronger cis heterodimers with members of different subfamilies, particularly γ C3 and/or γ C5, compared to their homodimeric and within-subfamily interactions. γ C3 also formed stronger heterodimers with α C2 than with itself or γ C5. Of note, α C2 and γ C5 both form strong cis homodimers with K_D s of 8.9 and 18.4 μ M, respectively, as determined from AUC experiments (**Figure 4—source data 1**), a magnitude similar to many of their heterodimeric interactions of 11.5 and 6.9–18.2 μ M, respectively (**Figure 4B**).

In the next section, we rationalize cis-binding preferences in terms of the structural properties of cis dimers.

The asymmetric cis dimer interface and cis-binding specificity

The crystal structure of the γ B7 cis dimer revealed an asymmetric interaction, with the dimer formed by one protomer engaging using surface of both EC5 and EC6 and one protomer engaging using only EC6 (**Goodman et al., 2017**) with regions of EC6 overlapping in both EC5–6 and the EC6-only interfaces for all cPcdh subfamilies (**Thu et al., 2014**; **Goodman et al., 2017**). The asymmetric nature

of the *cis* interaction implies that for each dimer interaction there are two possible arrangements: one with protomer '1' forming the EC5–6 side and protomer '2' forming the EC6-only side and the second where protomer '1' forms the EC6-only side and '2' the EC5–6 side. These two configurations are distinct with different residue:residue interactions. Alternate α -cPcdhs, which can only form the EC5–6 side of the *cis* dimer, require coexpression with a 'carrier' cPcdh from another cPcdh subfamily, which can form the EC6-only side of the *cis* dimer, for robust delivery to the cell surface (Thu et al., 2014; Goodman et al., 2017). Although α -cPcdhs and γ C4, which also requires a carrier for delivery to the cell surface, are likely to be extreme cases, sequence analysis alongside the low homodimerization ability of many cPcdh isoforms suggests many cPcdhs will more readily form one side of the *cis* interface than the other (Goodman et al., 2017).

We previously suggested that γ A-cPcdhs will prefer to form the EC6-only side of the interface since they have a poorly conserved EC5 interface and do not form strong homodimers in solution (Figure 4—source data 1; Goodman et al., 2017). The C-type cPcdh γ C3 also does not form *cis* homodimers in solution. However, as shown in Figure 4, γ A-cPcdhs form strong heterodimers with γ C3 with dissociation constants in the low-micromolar range (Figure 4B and Figure 4—figure supplement 1B). Structure-guided sequence analysis for the γ A4/ γ C3 dimer in both EC6-only and EC5–6 possible orientations, using the available crystal structures of the γ B7_{EC3–6} *cis* dimer and monomeric γ A4_{EC3–6} (Figure 5A and Figure 5—figure supplement 1), suggests that γ C3 prefers to form the EC5–6 side: γ C3 has a number of residue differences in interface residues that are conserved among β , γ A, and γ B cPcdhs (V/L555, R/K558, W/V562, and S/R595) that seem likely to disfavor the EC6-only side of the interface and favor the EC5–6 side (Figure 5—figure supplement 1B, C). Two of these residues, V555 and S595, result in a potential loss of EC6-only interface buried surface area and are shared with α -cPcdhs, which cannot occupy the EC6-only position (Goodman et al., 2017). Structural analysis further suggests that γ C3-specific residue R558 would not be well accommodated from the EC6-only side, potentially causing van der Waals clashes (Figure 5—figure supplement 1C). By contrast, from the EC5–6 side R558 is positioned to form an additional salt bridge with γ A4 residue E544 and a hydrogen bond with Y532, promoting dimer formation (Figure 5A; Figure 5—figure supplement 1B). γ A4 residue E544 is positioned to form this salt bridge due to the EC6 A/A' loop region adopting a different arrangement in the γ A4 crystal structure to that observed for γ B2 and γ B7 in their respective crystal structures (Goodman et al., 2016a; Goodman et al., 2017).

Based on our analysis, we generated mutants of both γ A4 and γ C3 targeting the EC6-only side of the interface and used size exclusion-coupled multiangle light scattering (SEC-MALS) to assess their preferred orientation on γ A4/ γ C3 heterodimerization. In SEC-MALS wild-type γ A4_{EC3–6} and γ C3_{EC3–6} behave as monomers when run alone, and form a dimer when mixed in equimolar amounts (Figure 5B; Figure 5—figure supplement 2A). The V560R mutation (γ B7 numbering, see methods for sequence alignment) is based on EC6-only impaired α -cPcdhs, and has been previously shown to block γ B6's homophilic *cis* interaction in solution (Goodman et al., 2017). γ A4 V560R did not dimerize with wild-type γ C3, whereas γ C3 V560R could still dimerize with wild-type γ A4 (Figure 5B). Therefore, impairing γ A4's EC6-only interface blocks γ A4/ γ C3 dimer formation while impairing γ C3's EC6-only interface does not (although the dimerization appears to be weaker compared to the wild-type γ A4/ γ C3 *cis*-interacting pairs). We also generated a γ C3-like mutant of γ A4, K558R, which also targets the EC6-only interface. Like γ A4 V560R, γ A4 K558R also did not dimerize with wild-type γ C3 in MALS and, when replicated, in SPR experiments (Figure 5B, Figure 5—figure supplement 2B). The reverse mutation in γ C3, R558K, inhibited dimerization with wild-type γ A4 (Figure 5B). Therefore, like the α -specific R560 residue, γ C3-specific R558 has distinct effects on dimerization when in γ A4 or γ C3, inhibiting heterodimerization when mutated into γ A4 but promoting heterodimerization in γ C3. Together these data suggest that the γ A4/ γ C3 dimer has a preferred orientation, with γ A4 predominantly occupying the EC6-only position and γ C3 the EC5–6 side. Our data also account for the fact that neither isoform homodimerizes in solution since the EC5–6 side would be impaired in the γ A4 homodimer while the EC6 side would be impaired in the γ C3 homodimer.

Next, we sought to test whether γ A4 and γ C3 preferentially adopt these specific positions in *cis* interactions with a γ B isoform. To accomplish this we generated mutants of γ B7 individually targeting the EC6-only interaction surface, γ B7 Y532G, and the EC5–6 side, γ B7 A570R, respectively (Goodman et al., 2017; Figure 4—source data 1). In SPR, γ B7 Y532G had only a small impact on γ A4 binding, while γ B7 A570R abolished γ A4 binding (Figure 5C). In contrast, γ B7 Y532G prevented γ C3 binding

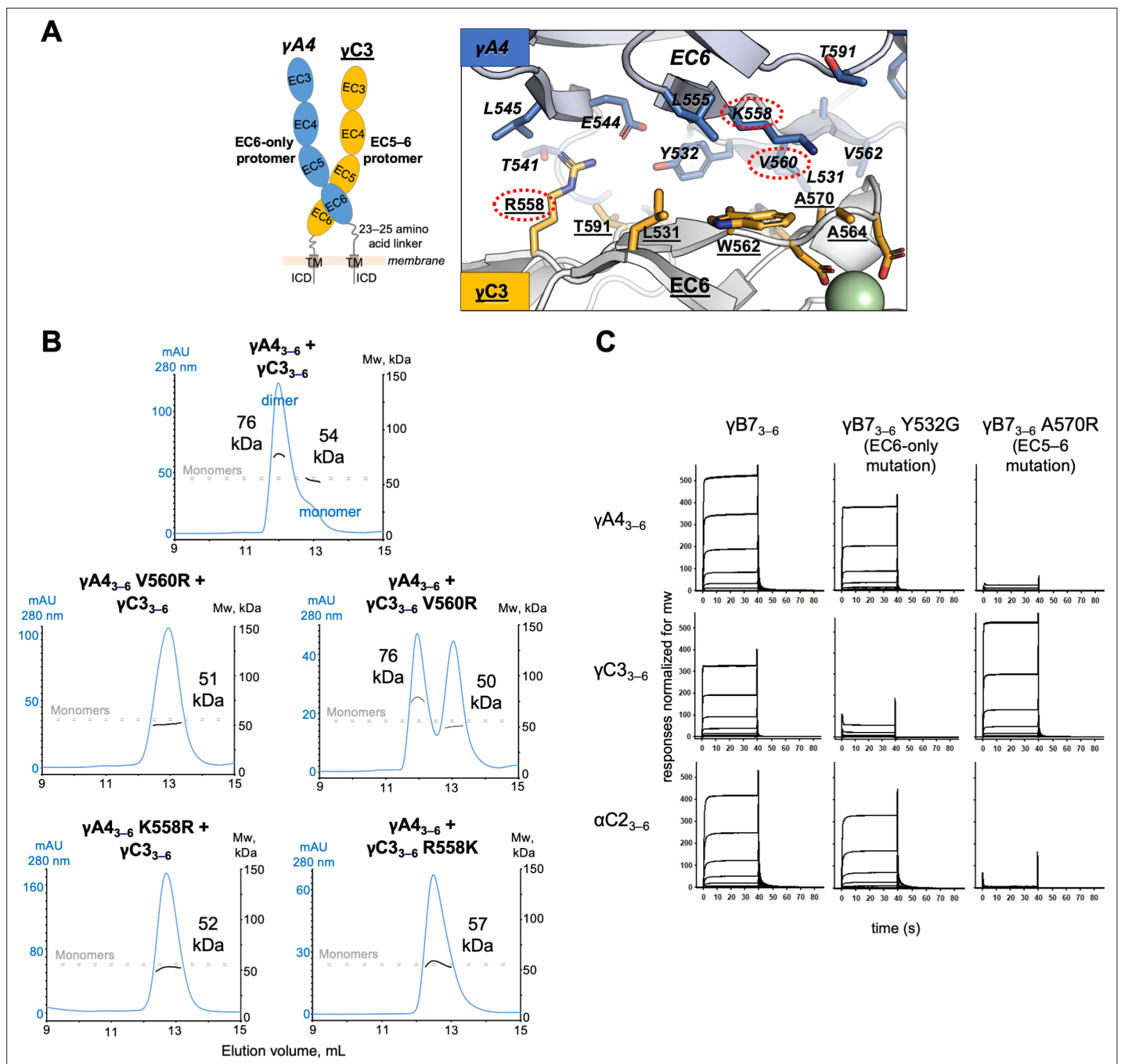


Figure 5. γ A4 preferentially forms the EC6-only side and γ C3 the EC5–6 side in *cis* dimers. **(A)** Structural model of γ A4/ γ C3 *cis* dimer based on γ B7_{EC3–6} *cis* dimer and γ A4_{EC3–6} crystal structures (PDBs: 5V5X and 5SZQ). γ A4 is shown adopting the EC6-only side (blue protomer) and γ C3 is shown adopting the EC5–6 side (yellow protomer). *Left*, schematic of the γ A4/ γ C3 EC3–6 *cis* dimer. *Right*, close-up view of the EC6:EC6 interface from the modeled *cis* dimer showing interfacial residue side chains. Bound calcium ions are shown as green spheres. Residues which were mutated in the panel B are circled in red. γ B7 crystal structure numbering is used for both γ A4 and γ C3 residues. See methods for γ A4 and γ C3 alignment. Please note the model shown here is solely for hypothesis generation, since it is unlikely to be completely accurate. See methods for further details of structural modeling. **(B)** *Top*, size exclusion-coupled multiangle light scattering (SEC-MALS) data for an equimolar mixture of wild-type γ A4_{EC3–6} and γ C3_{EC3–6} showing dimer formation. Plot shows size exclusion absorbance at 280 nm trace (left axis), molecular weight of the eluant peaks (right axis), and the monomer molecular weights of γ A4_{EC3–6} and γ C3_{EC3–6} measured by mass spectrometry – 54.5 and 56.5 kDa, respectively – as dashed gray lines. Average molecular weight of the molecules in the dimer and monomer eluant peaks are labeled. *Middle*, SEC-MALS data for V560R mutants, which target the EC6-only side of the interface. *Bottom*, SEC-MALS data for residue 558 mutants. The γ C3-like K558R mutation in γ A4 inhibits heterodimer formation with wild-type γ C3.

Figure 5 continued on next page

Figure 5 continued

Similarly, the γ A4-like R558K in γ C3 inhibits dimerization with wild-type γ A4. (C) SPR-binding profiles for γ B7_{EC3-6} wild-type and *cis* interface mutants flowed over three individual wild-type *cis* fragment surfaces. The two mutations specifically target one side of the *cis* interface.

The online version of this article includes the following figure supplement(s) for figure 5:

Figure supplement 1. Structure-guided sequence analysis of γ A4 and γ C3 *cis* interactions.

Figure supplement 2. γ A4 and γ C3 *cis* fragments behave as monomers in size exclusion-coupled multiangle light scattering (SEC-MALS) and mutating γ A4 to make it more like γ C3 prevents γ A4/ γ C3 *cis* heterodimerization.

while γ B7 A570R showed robust γ C3 binding (Figure 5C). These results suggest that γ A4/ γ B7 and γ C3/ γ B7 *cis* heterodimers also have preferred orientations with γ A4 and γ C3 maintaining their preferences for the EC6-only and EC5–6 positions, respectively. Additionally, SPR data for the γ B7 mutants over the α C2 surface suggest α C2 preferentially occupies the EC6-only side in α C2/ γ B7 dimers (Figure 5C). This is notable since α C2 forms robust *cis* homodimers and therefore, like γ B7, can presumably readily occupy both positions in its homophilic interactions, implying that the α C2/ γ B7 orientation preference could be specific to the particular heterodimer pairing. However, since this interpretation is based on a single mutation further interrogation of α C2's interactions would be required to be conclusive. A broader examination of orientation preferences among *cis* dimer pairings beyond those of molecules with weak *cis* homodimer affinities, such as γ A4 and γ C3 examined here, could be instructive.

Discussion

Trans specificity

The results of this study add to our current understanding of cPcdhs in a number of ways. First, they reveal a remarkable level of specificity in *trans* homophilic interactions since in no case was a heterophilic *trans* interaction detected in our SPR measurements. Prior data have clearly indicated that cPcdhs exhibit a preference for homophilic *trans* interactions but the extent of this specificity was not established in quantitative terms but were, rather, based on cell aggregation experiments. The SPR experiments with cPcdhs reported here show no evidence of cross-interaction between nonidentical cPcdh isoforms. This level of specificity is unusual for cell–cell recognition proteins, as significant intrafamily interactions are evident in most other families examined to date including type I cadherins (Katsamba et al., 2009; Vendome et al., 2014), type II cadherins (Brasch et al., 2018), DIPs and Dprs (Cosmanescu et al., 2018), sidekicks (Goodman et al., 2016b), and nectins (Harrison et al., 2012). Even the nonclustered δ -protocadherins, which are preferentially homophilic and utilize an antiparallel EC1–4 interface like the cPcdhs (Cooper et al., 2016; Harrison et al., 2020; Modak and Sotomayor, 2019), show heterophilic intra-family *trans* interactions, though they show no cross-reactivity with cPcdhs (Harrison et al., 2020).

High-fidelity homophilic interaction is a strict requirement of the chain-termination model for the barcoding of vertebrate neurons and has been accomplished through the exploitation of a multi-domain interface of almost 4000 Å² (Nicoludis et al., 2019) that enables the positioning of enough 'negative constraints' (Sergeeva et al., 2020) to preclude the dimerization of about 1600 heterophilic pairs of 58 mouse cPcdh isoforms (Rubinstein et al., 2017). Dscams accomplish the same task for thousands of isoforms by exploiting the combinatorics made possible by a three-domain interface where each domain interacts largely independently with an identical domain on its interacting partner (see discussion in Zipursky and Grueber, 2013). Although it is likely that Dscams dimerize with a comparable level of homophilic specificity to that of cPcdhs, the evidence is based on a semiquantitative ELISA-type assay of recombinant multimerized isoforms (Wojtowicz et al., 2007) and AUC experiments on a few select isoforms (Wu et al., 2012).

Cis interactions

Despite early evidence that *cis* interactions are promiscuous, the data reported here indicate that this generalization needs to be significantly refined. Functional mutagenesis studies have already established that alternate α cPcdhs and the C-type γ C4 do not form intrasubtype *cis* interactions and can only reach the cell surface when mediated by heterophilic *cis* interactions with members of

other subtype families (Goodman et al., 2017; Thu et al., 2014). The data presented in **Figure 4** indicate that this is an extreme example of quite general behavior: intrasubtype *cis* interactions are invariably weaker than intersubtype interactions. However, unlike α cPcdhs, most cPcdhs can reach the cell surface on their own. This includes β 1, all γ A-Pcdhs, and γ C3 which do not form measurable homodimeric *cis* interactions in our solution-based AUC experiments. We have attributed this to their presence on the restricted 2D surface of membranes which can promote *cis* dimerization (Wu et al., 2013) whereas biophysical experiments are carried out in a 3D solution environment (Goodman et al., 2016a). (There may of course be other, still undetermined, factors involved in cPcdh cell surface transport [Phillips et al., 2017].) Therefore, although our biophysical experiments demonstrate that intrasubtype *cis* interactions are comparatively weak and, in some cases undetectable in solution, intrasubtype *cis* dimers likely assemble when constrained in more native membrane environments. As such, while α cPcdhs and γ C4 are obligate participants in *cis* heterodimers, at least in their cell surface transport, our data show that the remaining cPcdhs are preferentially, although not exclusively, participants in *cis* heterodimers.

The *cis*-binding preferences indicated by our data can be largely understood in terms of the asymmetric interface discussed above. Specifically, different isoforms preferentially form one side of the *cis* dimer: for example, the EC6-only side for cPcdh- γ A4 and the EC5–6 side for cPcdh- γ C3. Homodimerization requires participation of single isoform on both sides of an interface posing challenges in the optimization of binding affinities since, in some cases, the same residue must participate in different intermolecular interactions. Given significant sequence conservation in all members of an alternate cPcdh subfamily (**Figure 4—figure supplement 3**) even intrasubfamily heterophilic interactions are more difficult to optimize relative to intersubfamily heterodimerization where there are no constraints on the two interacting surfaces. Additionally, the robust cell surface delivery of many cPcdhs in cells expressing only a single isoform also suggests that all carrier isoforms – β -, γ A-, and γ B-cPcdhs, plus C-types α C2, γ C3, and γ C5 – can fill both the EC6 and EC5–6 roles, as *cis* dimer formation is thought to be required for cell surface export (Goodman et al., 2017; Goodman et al., 2016a; ; Thu et al., 2014). Therefore side preferences are most likely not absolute for carrier cPcdh isoforms and may vary among individual isoform and/or subtype pairings.

Functional implications of cPcdh interactions

The functional role of precise *trans* homophilic specificity in ensuring high-fidelity discrimination between neuron self and nonself has been discussed previously (Rubinstein et al., 2017; Rubinstein et al., 2015) and is summarized above. It is an essential feature of the chain-termination model. The role of promiscuous *cis* interactions can also be understood in terms of this model in that *cis* promiscuity enables the formation of a large and diverse set of *cis* dimers that can only form long molecular zippers when all isoforms are matched. However, the results of this study reveal strong preferences for intersubgroup heterophilic interactions whose biological rationale is uncertain. cPcdhs from the three subfamilies have been shown to act cooperatively in certain neuronal contexts although whether this relates to their *cis* interactions is unknown (Hasegawa et al., 2016; Ing-Estevés et al., 2018).

One possible advantage of weak homophilic *cis* interactions would be to ensure that once reaching the cell surface a diverse set of *cis* dimers forms. This explanation implicitly assumes that most isoforms (except for α -Pcdhs and γ C4) reach the surface as homodimers that must then quickly dissociate and form more stable heterodimers. Another explanation posits that homotypic zippers consisting solely of *cis* homodimers are kinetically easier to form than heterotypic zippers since in a homotypic zipper, either ‘wing’ of the new *cis* dimer can form *trans* interactions with the wing at the chain terminus. In contrast, in a heterodimeric zipper, only one wing can form homophilic interactions with the chain terminus (**Figure 1D**). A preference for homotypic zippers would then reduce the diversity required in the chain-termination model since, in this model, it is essential that all isoforms be incorporated into a growing zipper. The formation of long homotypic zippers might lead to a repulsive phenotype even when mismatches are present.

However, these explanations would not fully account for interfamily heterophilic preferences. One possibility is suggested by the observation that C-types are often highly expressed compared to alternate cPcdhs, for example in Purkinje cells (Esumi et al., 2005; Kaneko et al., 2006). To ensure sufficient diversity in growing zippers, it would then be important to ensure that zippers that are formed are not overly enriched in C-type isoforms as would be accomplished through preferential heterophilic

cis interactions. This same logic would also pertain to alternate cPcdhs in cases where one subfamily is more heavily expressed than another.

C-type cPcdhs have different functions than alternate cPcdhs and these are reflected in different expression patterns. For example, α 2 can be alone responsible for tiling (Chen et al., 2017). (Of note, in the chain-termination model, a completely homophilic zipper is sufficient to initiate self-avoidance facilitating tiling.) On the other hand, γ 4, which has a unique and crucial role in neuronal survival (Garrett et al., 2019), requires coexpression with another cPcdh isoform for robust cell surface expression and therefore is likely unable to act in isolation (Thu et al., 2014). Furthermore, as detailed above, γ 4 has a much weaker *trans* interaction affinity than any other cPcdh isoform measured to date, although it is still able to mediate cell aggregation when delivered to the cell surface (Thu et al., 2014). The presence of E78 appears in large part to be responsible for this weak affinity. It is unclear whether γ 4's weak *trans* affinity plays any functional role, although a weak homodimer interaction may facilitate extracellular interactions with other, currently unidentified, proteins. More generally, it seems likely that different intracellular interactions account for the specialized functions of C-type Pcdhs. The cytoplasmic domain plays an important role in the activation of Wnt, WAVE, and other signaling cascades (Chen et al., 2009; Fukuda et al., 2008; Keeler et al., 2015; Mah and Weiner, 2017; Onouchi et al., 2015; Pancho et al., 2020). In some cases, the cytoplasmic domains of a subset or even a single cPcdh isoform activates a specific signaling cascade. For example, cPcdh γ 3 is the only isoform able to interact and inhibit Axin1, a Wnt pathway activator (Mah et al., 2016). Of note, γ -cPcdh intracellular domains consist of a C-terminal constant region common to all γ isoforms (including the three γ C-types) and a membrane-proximal variable region consisting of ~100 residues that could account for the unique intracellular interactions and signaling of individual isoforms. Additionally, it is possible that extracellular interactions to molecules from other families, such as Neurotrogins, may account for some distinctions in function (Molunby et al., 2017; Steffen et al., 2021).

Overall, the results of this study demonstrate the remarkable tuning of the interactions among cPcdh family members: homophilic *trans* interactions are remarkably specific despite the high level of sequence identity among family members while *cis* interactions, though somewhat promiscuous, also appear designed to have binding preferences of still uncertain function. These binding properties match requirements of the 'isoform-mismatch chain-termination model' for neuronal self- vs nonself-discrimination in which all expressed cPcdh isoforms assemble into intercellular zippers formed by alternating promiscuous *cis* and matched *trans* interactions with assembly size dictated by the presence or absence of mismatched isoforms. It remains to be seen whether such assemblies can be observed in vivo and how they control downstream signaling pathways.

Materials and methods

Protein production and purification

cDNAs for mouse cPcdh ectodomain fragments, excluding the predicted signal sequences, were cloned into a p α SHP-H mammalian expression vector (a kind gift from Daniel J. Leahy, Johns Hopkins University) modified with the human binding immunoglobulin protein (BiP; MKLSLVAAMLLLLSAARA) signal sequence and a C-terminal octa-histidine tag (Rubinstein et al., 2015). The signal sequences were predicted using the SignalP 4.0 server (Petersen et al., 2011). Point mutations were introduced into cDNA constructs using the KOD hot start polymerase (Novagen) following the standard Quik-change protocol (Stratagene).

Suspension-adapted HEK293 Freestyle cells (Invitrogen) in serum-free media (Invitrogen) grown and maintained at 37°C and 10% carbon dioxide were used for protein expression. FreeStyle 293F cell line has been authenticated and verified negative for mycoplasma using PCR testing (Thermo Fisher). The plasmid constructs were transfected into cells using polyethyleneimine (Polysciences Inc) (Baldi et al., 2012). Media was supplemented with 10 mM CaCl₂ 4 hr after transfection. Conditioned media was harvested ~6 days after transfection and the secreted proteins were purified using batch nickel-nitrilotriacetic acid (Ni-NTA) affinity chromatography followed by size exclusion chromatography over Superdex 200 26/60 column (Cytiva) on an AKTA pure fast protein liquid chromatography system (Cytiva). Purified proteins were concentrated to >2 mg/ml in 10 mM Tris-Cl, pH 8.0, 150 mM NaCl, 3 mM CaCl₂, and 100–250 mM imidazole pH 8.0 and stored at 4°C for short-term use or flash frozen in liquid nitrogen for long-term storage at –80°C.

Constructs encoding biotinylated cPcdh fragments for immobilization in SPR experiments were prepared by insertion of an Avi-tag (GLNDIFEAQKIEWHE)-encoding sequence between the octahistidine tag and stop codon. These were cotransfected with a plasmid encoding the biotin-Ligase BirA from *E. coli* (Lys2–Lys321) with a BiP signal sequence and a C-terminal endoplasmic reticulum-retention signal (DYKDEL) (*Barat and Wu, 2007*). The expression and BirA plasmids were mixed at a 9:1 ratio for transfection and 50 μ M Biotin (Sigma) was added to the media 4 hr post-transfection. Purification was carried out exactly as for the nonbiotinylated constructs and biotinylation was confirmed by western blot using NeutrAvidin-HRP (Thermo Fisher).

Sedimentation equilibrium AUC

Protein	Imidazole pH 8.0 (mM)	Spin speeds (rpm)
α 4 EC1–5	100	9000, 11,000, 13,000, 15,000
α 7 EC1–5 L301R	100	9000, 11,000, 13,000, 15,000
α 12 EC1–5 (<i>poorly behaved</i>)	200	11,000, 14,000, 17,000, 20,000
γ B4 EC1–5	200	11,000, 14,000, 17,000, 20,000
γ B5 EC1–4-AVI	200	11,000, 14,000, 17,000, 20,000
γ C5 EC1–5 S116R	200	11,000, 14,000, 17,000, 20,000
β 6 EC1–4	100	9000, 11,000, 13,000, 15,000
β 6 EC1–4-AVI tag	200	11,000, 14,000, 17,000, 20,000
β 6 EC1–4 R41N	200	11,000, 14,000, 17,000, 20,000
β 6 EC1–4 S117I	200	11,000, 14,000, 17,000, 20,000
β 6 EC1–4 L125P	200	11,000, 14,000, 17,000, 20,000
β 6 EC1–4 E369K	200	11,000, 14,000, 17,000, 20,000
β 6 EC1–4 Y371F	200	11,000, 14,000, 17,000, 20,000
β 6 EC1–4 R41N/S117I (<i>precipitates</i>)	200	11,000, 14,000, 17,000, 20,000
β 6 EC1–4 R41N/E369K	200	11,000, 14,000, 17,000, 20,000
β 6 EC1–4 S117I/L125P	200	11,000, 14,000, 17,000, 20,000
β 6 EC1–4 R41N/S117I/L125P	200	11,000, 14,000, 17,000, 20,000
β 6 EC1–4 R41N/S117I/E369K	200	11,000, 14,000, 17,000, 20,000
β 6 EC1–4 R41N/E369K/Y371F	200	11,000, 14,000, 17,000, 20,000
β 6 EC1–4 R41N/S117I/L125P/ E369K/Y371F	200	11,000, 14,000, 17,000, 20,000
β 1 EC3–6	200	12,000, 16,000, 20,000, 24,000
β 6 EC1–6	250	9000, 11,000, 13,000, 15,000
β 9 EC3–6	200	11,000, 14,000, 17,000, 20,000
γ A3 EC3–6	200	11,000, 14,000, 17,000, 20,000
γ A9 EC3–6	200	11,000, 14,000, 17,000, 20,000
γ B7 EC3–6 A570R	200	13,000, 17,000, 21,000, 25,000
α C2 EC3–6-AVI tag	200	11,000, 14,000, 17,000, 20,000
γ C5 EC2–6	250	9000, 11,000, 13,000, 15,000
γ C4 EC1–4	250	11,000, 14,000, 17,000, 20,000
γ C4 EC1–4 D290A	250	11,000, 14,000, 17,000, 20,000
γ C4 EC1–4 D290N	250	11,000, 14,000, 17,000, 20,000

Continued on next page

Continued

Protein	Imidazole pH 8.0 (mM)	Spin speeds (rpm)
γ C4 EC1–4 E78A	250	11,000, 14,000, 17,000, 20,000
γ C4 EC1–4 E78Q	250	11,000, 14,000, 17,000, 20,000
γ C4 EC1–4 S344R	250	11,000, 14,000, 17,000, 20,000

Experiments were performed in a Beckman XL-A/I analytical ultracentrifuge (Beckman-Coulter, Palo Alto CA, USA), utilizing six-cell centerpieces with straight walls, 12-mm path length and sapphire windows. Protein samples were dialyzed overnight and then diluted in 10 mM Tris-Cl, pH 8.0, 150 mM NaCl, 3 mM CaCl₂ with 100–250 mM imidazole pH 8.0, as detailed in the above table. The samples were diluted to an absorbance of 0.65, 0.43, and 0.23 at 10 and 280 nm in channels A, B, and C, respectively. For each sample, buffer was used as blank. The samples were run in duplicate at four speeds as detailed in the above table. The lowest speed was held for 20 hr then four scans were conducted with 1-hr interval, the subsequent three speeds were each held for 10 hr followed by four scans with 1-hr interval each. Measurements were taken at 25°C, and detection was by UV at 280 nm or interference. Solvent density and protein ν -bar at both temperatures were determined using the program SednTerp (Alliance Protein Laboratories, Corte Cancion, Thousand Oaks, CA, USA). The molecular weight of each protomer used in AUC experiments was determined by MALDI mass spectrometry. For the calculation of dimeric K_D and apparent molecular weight, all data were used in a global fit, using the program HeteroAnalysis (<http://www.biotech.uconn.edu/auf>). The calculation of the tetramer K_D s was done with the program Sedphat (<http://www.analyticalultracentrifugation.com/sedphat/index.htm>).

SPR binding experiments

SPR-binding experiments were performed using a Biacore T100 biosensor equipped with a Series S CM4 sensor chip, immobilized with NeutrAvidin over all four flow cells. NeutrAvidin immobilization was performed in HBS-P (HEPES-Buffered Saline-P20) buffer, pH 7.4 at 32°C, over all four surfaces using amine-coupling chemistry as described in *Katsamba et al., 2009*, resulting in approximately 10,000 RU of NeutrAvidin immobilized (*Katsamba et al., 2009*). Binding experiments were performed at 25°C in a running buffer containing 10 mM Tris-Cl, pH 8.0, 150 mM NaCl, 3 mM CaCl₂, 20 mM imidazole, 0.25 mg/ml BSA (Bovine Serum Albumin), and 0.005% (vol/vol) Tween-20 unless otherwise noted.

C-terminal biotinylated fragments were tethered over individual NeutrAvidin-immobilized flow cells (shown in the left column of each *Figures 2, 4, and 5C, Figure 2—figure supplement 1, Figure 2—figure supplement 2B, Figure 4—figure supplement 1, and Figure 5—figure supplement 2B*) at 2300–3000 RU, depending on the experiment, using a flow rate of 20 μ l/min. A NeutrAvidin-immobilized flow cell was used as a reference in each experiment to subtract bulk refractive index changes. The analytes tested in each experiment are listed at the top row. All analytes (with exceptions for the *cis*-interacting pairs γ C3_{3–6}/ β 9_{3–6}, in both orientations, and β 6_{1–6}/ γ C3_{3–6} in *Figure 4A*, discussed below) were tested at six concentrations ranging between 24, 8, 2.667, 0.889, 0.296, and 0.099 μ M, prepared using a threefold dilution series. γ C3_{3–6} binding over β 9_{3–6} (*Figure 4A*) was tested at five concentrations from 8 to 0.099 μ M.

For all experiments, analyte samples were injected over the captured surfaces at 50 μ l/min for 40 s, followed by 180 s of dissociation phase, a running buffer wash step and a buffer injection at 100 μ l/min for 60 s. Protein samples were tested in order of increasing concentration, and within the same experiment the entire concentration series was repeated to confirm reproducibility. Every three binding cycles, buffer was used as an analyte instead of a protein sample to double reference the binding responses by removing systematic noise and instrument drift. The resulting binding curves were normalized for molecular weight differences according to data provided by mass spec for each molecule. The data were processed using Scrubber 2.0 (Biologic Software). To provide an estimate of the number of possible heterophilic binding pairs, we have used a cutoff of 40 RU, which is the lowest signal that can be observed for a homodimeric *cis* fragment pair, γ B2_{3–6}.

In *Figure 4A*, β 6_{1–6} and β 9_{3–6} were tested over γ C3_{3–6} at six concentrations ranging from 900 to 3.7 nM, which is 27-fold lower than the other interactions, prepared using a threefold dilution series

in a running buffer containing increased concentrations of imidazole (100 mM) and BSA (0.5 mg/ml) to minimize nonspecific interactions. For these two interactions, although analyte samples were injected over the captured surfaces at 50 $\mu\text{l}/\text{min}$ for 40 s, the dissociation phase was monitored for 300 s to provide additional time for complex dissociation. Nevertheless, higher analyte concentrations produced binding profiles that were not reproducible, most likely due to the fact that bound complexes could not dissociate completely at these higher concentrations.

For the calculation of heterophilic K_D s for the monomeric *cis* fragments β_{1-3-6r} , γA_{4-3-6r} , γA_{9-3-6r} and γC_{3-3-6} over each of the six surfaces, except β_{9-3-6r} , the duplicate binding responses were fit globally, using an 1:1 interaction model and a single K_D was calculated as the analyte concentration that would yield 0.5 R_{max} and a fitting error, indicated in brackets. K_D s lower than 24 μM were calculated using an independent R_{max} . For K_D s greater 24 μM , the R_{max} was fixed to a global value determined by the R_{max} of a different cPcdh analyte tested over the same surface during the same experiment that showed binding above 50% and therefore produced a more accurate R_{max} . For K_D s > 50 μM , a lower limit is listed since at the analyte concentrations used (0.098–24 μM), accurate K_D s could not be determined, even when the R_{max} is fixed. NB (no binding) represents interactions that did not yield any binding signal. The binding curves of γC_{3-3-6} over the β_{9-3-6r} did not come to equilibrium during the time-course of the experiment, so a kinetic analysis was performed to calculate a K_D (**Figure 4—figure supplement 1A**). Binding of γC_{3-3-6} was tested using a concentration range of 900–0.411 nM prepared using a threefold dilution series in a running buffer containing increased concentrations of imidazole (100 mM) and BSA (0.5 mg/ml) to minimize any nonspecific interactions. Protein samples were injected over the captured surfaces at 50 $\mu\text{l}/\text{min}$ for 90 s, followed by 420 s of dissociation phase, a running buffer wash step and a buffer injection at 100 $\mu\text{l}/\text{min}$ for 60 s. Protein samples were tested in order of increasing concentration in triplicate to confirm reproducibility. Every three binding cycles, buffer was used as an analyte instead of a protein sample to double reference the binding responses by removing systematic noise and instrument drift. The binding data were analyzed using an 1:1 interaction model to calculate the kinetic parameters and the K_D .

K562 cell aggregation assays

Full-length cPcdhs β_6 and β_8 cDNAs were cloned into the pMax expression vectors encoding C-terminal mCherry- or mVenus-tagged cPcdh proteins, then transfected into K562 cells (ATCC CCL243) as previously described (**Goodman et al., 2017; Thu et al., 2014**). K-562 bone marrow chronic myelogenous leukemia cell line has been authenticated and verified negative for mycoplasma using PCR testing (ATCC). Point mutants were generated using the QuikChange method (Stratagene). In brief, K562 cells were cultured at 37°C with 5% CO_2 in Dulbecco's modified Eagle medium with GlutaMAX (GIBCO) supplemented with 10% fetal bovine serum and 1% penicillin–streptomycin for 2 days. Next, cells were counted, centrifuged, and resuspended at a density of 1.5×10^4 cells/ μl in SF Cell Line 4D-Nucleofector Solution SF with supplement according to the manufacturer's instructions (Lonza). 2 μg of each Pcdh expression construct were transfected into 20 μl of the K562 cell suspension by electroporation using an Amaxa 4D-Nucleofector (Lonza). Transfected cells were transferred to a 24-well plate in 500 μl of medium per well and incubated overnight at 37°C and 5% CO_2 . Cells then were mixed, reincubated with gentle rocking for 4 hr, then imaged with an Olympus IX73 fluorescent microscope to determine the extent of aggregation.

Size exclusion-coupled multiangle light scattering

SEC-MALS experiments were performed using a Superdex 200 Increase 3.2/300 size exclusion column on an AKTA FPLC system (Cytiva) coupled to inline static light scattering (Dawn Heleos II, Wyatt Technology), differential refractive index (Optilab rEX, Wyatt Technology), and UV detection. Purified cPcdh proteins were diluted to 18 μM in running buffer (150 mM NaCl, 10 mM Tris–Cl, pH 8, 3 mM CaCl_2 , 200 mM imidazole, pH 8) and 50 or 100 μl samples were run at a flow rate of 0.5 ml/min at room temperature. Mixtures of cPcdh fragments were prepared in the same buffer at final concentrations of 18 μM for each protein and run under the same conditions. Data were analyzed using ASTRA software (Wyatt Technologies).

During SEC-MALS experiments, a dimer/monomer equilibrium is established as proteins move through the size exclusion chromatography column, which is influenced by the K_D of the interaction. The concentrations used in the current experiments (18 μM for each cPcdh fragment), although above

the K_D of 3 μ M for the γ C3/ γ A4 *cis* interaction, are not sufficiently high for all the *cis* fragments to be bound into heterodimers, leaving a significant population of molecules as monomers, resulting in apparent molecular weights of \sim 76 kDa for the dimeric species compared to the predicted molecular weight for a dimer of \sim 108 kDa.

X-ray crystallography

Crystallization screening of γ C4₁₋₄ using the vapor diffusion method yielded two protein crystal forms: The first crystal form crystals were grown using a protein concentration of 7 mg/ml in 10% (wt/vol) PEG8000, 20% ethylene glycol, 10% Morpheus Amino Acids (Molecular Dimensions), and 0.1 M Morpheus Buffer System 2 (Hepes/MOPS buffer; Molecular Dimensions), pH 7.5. No additional cryoprotection was required for this crystal form. The second crystal form crystals were grown using a protein concentration of 7 mg/ml in 1 M LiCl, 0.1 M Mes pH 6.0, and 10% (wt/vol) PEG 6000. The crystal used for data collection was cryoprotected in the crystallization condition plus 30% (wt/vol) glycerol. X-ray diffraction data for each crystal form were collected at 100 K from single crystals at Northeastern Collaborative Access Team (NE-CAT) beamline 24ID-E at the Advanced Photon Source, Argonne National Laboratory.

γ C4₁₋₄ crystal form 1: diffraction anisotropy and pseudosymmetry

The X-ray diffraction data for the first crystal form showed strong diffraction anisotropy, with relatively strong diffraction along c^* and much weaker diffraction along a^* and b^* (**Figure 3—figure supplement 1A**). These data were therefore truncated using ellipsoidal limits with using a 3.0 F/sigma cutoff along each of the three principal crystal axes as implemented in the UCLA Diffraction Anisotropy Server (**Strong et al., 2006**) to 4.6/3.9/3.5 Å. The completeness within the applied ellipsoidal resolution limits was 96.8% (**Figure 3—source data 1**).

γ C4₁₋₄ crystal form 1: crystal structure phasing and refinement

The γ C4₁₋₄ crystal structure was solved by molecular replacement using Phaser (**McCoy et al., 2007**), implemented in CCP4 (**Winn et al., 2011**). The γ C5_{EC1-3} crystal structure (PDB: 4ZPO) modified using a sequence alignment to γ C4 with Phenix's MRage program (**Liebschner et al., 2019**) was used as a search model. Following an initial round of rigid body refinement in Phenix (**Liebschner et al., 2019**) the EC domain 4 from the α 7_{EC1-5} crystal structure (PDB: 5DZV) was manually placed into the electron density map, using structural alignment to the EC1–3 regions as a guide. The resulting model was subjected to a further round of rigid body refinement. At this stage there was clear difference density for the interdomain calcium ions and covalently linked glycans not present in the models. Iterative model building using Coot (**Emsley et al., 2010**) and maximum-likelihood refinement using Phenix (**Liebschner et al., 2019**) was subsequently conducted. The higher resolution (2.4 Å) crystal form two crystal structure (see below) was used as a reference model in later rounds of iterative model building and refinement to guide the local geometry choices in this lower resolution structure. Final refinement statistics are given in **Figure 3—source data 1**.

γ C4₁₋₄ crystal form 2: data processing, phasing, and refinement

The γ C4₁₋₄ crystal form two dataset was indexed using XDS (**Kabsch, 2010**) and scaled using AIMLESS (**Evans and Murshudov, 2013**). The data were spherically truncated with high resolution limit of 2.4 Å. Data collection statistics are given in **Figure 3—source data 1**.

The γ C4₁₋₄ crystal form two crystal structure has two molecules in the asymmetric unit was solved by molecular replacement using Phaser (**McCoy et al., 2007**), implemented in Phenix (**Liebschner et al., 2019**), using the EC2–3 portion of the *trans* dimer from the γ C4₁₋₄ crystal form one crystal structure early in refinement as a search model. The molecular replacement solution was then subjected to an initial round of rigid body refinement using Phenix, followed by two rounds of model building in Coot (**Emsley et al., 2010**) and maximum-likelihood refinement in Phenix. The two EC4 domains were then manually placed in the electron density and subjected to rigid body refinement. Following a further two iterative rounds of model building and refinement the two EC1 domains were manually placed. Iterative model building and refinement continued yielding the final crystal structure whose statistics are given in **Figure 3—source data 1**.

Structure analysis

Buried surface areas were calculated using 'Protein interfaces, surfaces and assemblies' service (PISA) at the European Bioinformatics Institute (http://www.ebi.ac.uk/pdbe/prot_int/pistart.html) (*Krissinel and Henrick, 2007*) and are given as the change in accessible surface area over both protomers. Root mean square deviations over aligned C α atoms (RMSDs) between structures were calculated using Pymol (Schrödinger, LLC). Crystal structure figures were made using Pymol (Schrödinger, LLC).

Sequence analysis

Multiple sequence alignments were generated using Clustal Omega (*Sievers et al., 2011*) and visualized using ESPript3.0 (*Robert and Gouet, 2014*). Sequence logos were generated from multiple sequence alignments using WebLogo3 (*Crooks et al., 2004*).

Amino acid sequence alignment of cPcdhs γ B7, γ A4, and γ C3 EC1–6 regions

CLUSTAL O(1.2.4) multiple sequence alignment

γ B7	-QPVRYSIPEELDRGSVVGKLAQDLGLSVLEVSARKLRVS--AEKLFHVSVDSESGDLLVK	57
γ A4	-EQIRYSVPEELERGSVVGNLAAADLGLPEGKLAERGVRIVSRGKTQLFALNPRSGSLVTA	59
γ C3	STIIHYEILEERERGFVGNVVDLGLDLGSLARRLRVVGASRRFFEWNWETGEMFVN	60
	::*.: ** :** **:: ****. :. : * :*: .. * :: :*:...	
γ B7	DRIDREQICKGRRKCELQLEAVLENPLNIFHVVEIEDVNDHAPQFPKDEINLEISESDS	117
γ A4	GRVDREGLCDRSPKCTANLEILLEDKVRILAIEVEIIDVNDNAPSFGAQQREIKVAESEN	119
γ C3	DRLDREELCGTLPSCVTLELVVENPLELFSAEVVVQDINDNNSPFTGEMKLEISEALA	120
	.*:*** :* . * ** ::*: ::*: * : *:*: * * : : ::*: *	
γ B7	PGARTILESAKDLDIGMNSLSKYQLSPNDYFLLLKDNPDGSKYPELELQKMLDREAEST	177
γ A4	PGTRFPLPEAFDLDIGVNALQGYQLSSNDHFSLDVQSGPDGIKYPELVLENALDREEEAV	179
γ C3	PGTRFPLESAHDPDVGNSLQTYELSHNEYFALRVQTRFDGTYAELVLERALDWEREPS	180
	**.* * . * * *:* *:* *:* * * : ** ** * * *:. * * * *	
γ B7	HHLMLTAVDGGDPPRTGTTQLRIRVVDANDNRPVFSQDVYRVRLPEDLPPGTTVLRKAM	237
γ A4	HHLVLTAFDGGDPVRSQTATIQTTLVDTNDNAPVFTQPEYHISVKENLPVGTLLTIKAT	239
γ C3	VQLVLTALDGGTPARSATLPIRITVLDANDNAPAFNQSLYRVRVEDAPPGRVAQVLAT	240
	::*:*:*.* ** * *:* * :. :*:*** *:* * * : : * : * ** : : *	
γ B7	DQDEGINAEFTYSFLGV-ANK--AQFSLDPITGDIVTRQSLDFEEVEQYTTIDVEAKDRGS	294
γ A4	DPDEGVNGEVTYSFRNV-REKISQLFQLNSLTGDIIVLGLDYEDSGFYDVDVEAHDGPG	298
γ C3	DLDEGLNGEIVYSFGSHNRAGVRELFALDLVTGVLTIKGRLDFFEDTKLHEIYIQAKDKGA	300
	* ***:.*.*.*** . * * : ** :. **:* : : :*: * *	
γ B7	--LSSQCKVIIIEVLNDNRPEIIITSLSDQISEDSPSGTVVVALFKVRDRDSGENAEVMC	352
γ A4	--LRARSKVLVTVLDVNDNAPEVTVTSLTSSIQEASSPGTVIALFNVDSDSGENGLVTC	356
γ C3	NPEGAHCKVLVEVVDVNDNAPEITVTSVSPVPEDAPLGTVIALLSVTDLDAGENGLVTC	360
	::*:*:*: *:* ** * * : ** : . : * : * **:*:* * * *.* * *	
γ B7	SLSGNNPFKIHSSSNYYKLVTDSDILDREQTPGYNVITATDRGKPPSSSTITLNVAD	412
γ A4	SIPDNLPFRLEKTYGNYHRLLIHRTLDRREVSDYNITITATDQGTPLSTETYISLQVVD	416
γ C3	EVPPGLPFSLTSSLKNYFTLKTSAALDRETMPEYNLSITARDSGIPSLALTTVKVQVSD	420
	:: . ** : .: ** . * **** **:*:* * * * ** : * :*: * *	
γ B7	VNDNAPVFQQAYLINVAENNPQGSITQVKAWDPDVGSNGLVSYIIASDLEPKALSSF	472
γ A4	INDNPPFTTHASYSAYIPENNPRGASILSITAQDPDGENAQVIYLSLEDTIQGAPMSSY	476
γ C3	INDNPPQSSQSSYDVYVEENNLPGVPILNLSVWDPDAPPNARLSFFLLEPGAETGLVSRV	480
	::** * : : * : ** * . * ** * . : : : : : * :	
γ B7	VSVNQDSGVVYAQRAFDHEQIRSFQLTLQARDQGSPALSANVSMRVLVDDRNDNAPRVLY	532
γ A4	VSINSNTGVLYALRSFDYEQFDLKLVTARDSGTTPPLSSNVLSLSVLDQNDNTPEILY	536
γ C3	FTINRDNGVLTTLVPLDYEDQREFQLTAHINDGGTPVLATNISVNVFVTDNRNDAPQVLY	540
	::* : ** : : *:* : :*: * * * *:*:* : * *:*:*:*:*:	
γ B7	PTLEPDGSALFDMVPRAAEPGYLVTKVVAVDADSGHNAWLSYHVLQASDPGLFSLGLRTG	592
γ A4	PTIPTDGSTGVELTPRSADPGYLVTKVVAVDKDSQNAWLSYRLLKASEPGLFSVGLHTG	596
γ C3	PR--PGQSSVEMLPRGTAAGHVSRVVGWDADAGHNAWLSYSLLGAPNQSLFAVGLHTG	597

```

*   *.: .:: **.: *:::***. * *:***** :* * : .**:**:**
γB7  EVRTARALSDKDAARQRLLVAVRDGGQPPLSATATLLLVFADSLQE           638
γA4  EVRTARALLDRDALKQSLVVTVDHGGQPPLSATVTLTIAVSDNIPD           642
γC3  QISTARPIQDTSRQILTVLISDSGEPDLLSTATLTVSVTEESPE           643
:: *** : * * : * * * : * * * **:*.* : .:.. :

```

Structure-based sequence analysis of the γ A4/ γ C3 interaction

Since both γ A4₃₋₆ and γ C3₃₋₆ are monomeric in solution but form a robust heterodimer when mixed (in SPR, AUC, and SEC-MALS) we hypothesized that these molecules might have opposing *cis* interaction side preferences. To facilitate hypothesis generation on the nature of their *cis* heterodimer interaction we modeled the two possible γ A4/ γ C3 *cis* dimers: one with γ A4 occupying the EC6-only position and γ C3 the EC5-6 position; and the second with γ C3 in the EC6-only position and γ A4 in the EC5-6 position. To do this the monomeric γ A4_{EC3-6} crystal structure (PDB: 5SZQ) was structurally superimposed over EC6 domains with the EC6-only protomer from the γ B7_{EC3-6} *cis* dimer crystal structure (PDB: 5V5X; RMSD 0.7 Å over 91 aligned C α s) or over EC5-6 domains with the EC5-6 protomer (RMSD 1.0 Å over 194 aligned C α s). Since γ A4 and γ B7 are so structurally similar in their EC5-6 regions modeling γ A4's *cis* interactions in this manner as a basis for hypothesis generation seemed reasonable. The only region of significant structural deviation within the EC5-6 regions between γ A4 and γ B7 is in the EC6 A-A' loop region which has a peripheral role in the EC6-only protomer interface. For modeling γ C3 we used computational mutagenesis of the γ B7 structure selecting the best-fit rotamer for each amino acid from the Dunbrack rotamer library (*Shapovalov and Dunbrack, 2011*), implemented in UCSF Chimera (*Pettersen et al., 2004*). No energy minimization was conducted and the models are intended only for use in hypothesis generation.

Cis interface mutants

Our studies of Pcdh *cis* interactions we have found that mutagenesis of the *cis* interface commonly has a deleterious impact on protein expression levels in our system (*Goodman et al., 2017*). We assume this is because *cis* interaction is required for robust cell surface delivery/secretion (*Thu et al., 2014*), although this has not been specifically addressed in our HEK293 protein expression system.

To test our structure-guided hypotheses regarding γ A4 and γ C3s' *cis* interactions and side preferences as we tried to make a number of different *cis* interface mutants and were able to obtain four different mutants (see table below). Since protein yields were generally too low for AUC and SPR, MALS was used to study the impact of these mutants on γ A4/ γ C3 *cis* dimer formation.

Mutant protein (γ B7 numbering given in parentheses)	<i>Cis</i> interface side targeted	Protein expression in 25 ml test
γ C3 EC3-6 Y540G (Y532G equivalent)	EC6-only	No
γ C3 EC3-6 V560D (L555D equivalent)	EC6-only	No
γ C3 EC3-6 V565R (V560R equivalent)	EC6-only	Yes
γ C3 EC3-6 A575R (A570R equivalent)	EC5-6	No
γ C3 EC3-6 R563K (K558R equivalent)	Both	Yes
γ A4 EC3-6 Y536G (Y532G equivalent)	EC6-only	No
γ A4 EC3-6 L559D (L555D equivalent)	EC6-only	No
γ A4 EC3-6 V564R (V560R equivalent)	EC6-only	Yes
γ A4 EC3-6 A574R (A570R equivalent)	EC5-6	No
γ A4 EC3-6 K562R (K558R equivalent)	EC6-only	Yes
β 1 EC3-6 V563R (V560R equivalent)	EC6-only	No
β 1 EC3-6 S573R (A570R equivalent)	EC6-only	No
β 1 EC3-6 K561R (K558R equivalent)	EC5-6	No

Continued on next page

Continued

Mutant protein (γ B7 numbering given in parentheses)	Cis interface side targeted	Protein expression in 25 ml test
β 9 EC3–6 V563R (V560R equivalent)	EC6-only	No
β 9 EC3–6 A573R (A570R equivalent)	EC6-only	No
β 9 EC3–6 K561R (K558R equivalent)	EC5–6	No

Acknowledgements

We thank Surajit Banerjee for help with synchrotron data collection at the APS NE-CAT 24-ID-C/E beamlines, supported by NIH P41GM103403. This work was supported by the NIH (grants R01MH114817 to LS and R01DK106548 to RS), the National Science Foundation (grant MCB-1914542 to BH), the Israel Science Foundation (grant 1463/19 to RR), and the Israel Cancer Research Fund (grant ICRF 19-203-RCDA to RR).

Additional information

Funding

Funder	Grant reference number	Author
National Institutes of Health	R01MH114817	Lawrence Shapiro
National Institutes of Health	R01DK106548	Rosemary V Sampogna
National Science Foundation	MCB-1914542	Barry Honig
Israel Science Foundation	1463/19	Rotem Rubinstein
Israel Cancer Research Fund	ICRF19-203-RCDA	Rotem Rubinstein

The funders had no role in study design, data collection, and interpretation, or the decision to submit the work for publication.

Author contributions

Kerry Marie Goodman, Conceptualization, Data curation, Formal analysis, Writing – original draft, Writing – review and editing, Cloned, expressed, purified and crystallized proteins; Phinikoula S Katsamba, Data curation, Formal analysis, Methodology, Writing – review and editing, Writing – original draft, Performed and analyzed SPR experiments; Rotem Rubinstein, Writing – review and editing; Göran Ahlsén, Data curation, Formal analysis, Performed and analyzed the analytical ultracentrifugation and multi-angle light scattering experiments; Fabiana Bahna, Data curation, Formal analysis, Cloned, expressed, purified and crystallized the proteins; Seetha Mannepalli, Data curation, Formal analysis, Cloned, expressed, purified and crystallized the proteins; Hanbin Dan, Data curation, Formal analysis, Performed and analyzed the cell aggregation experiments; Rosemary V Sampogna, Data curation, Formal analysis, Funding acquisition, Performed and analyzed the cell aggregation experiments; Lawrence Shapiro, Conceptualization, Funding acquisition, Writing – original draft, Writing – review and editing, Formal analysis, Designed experiments, analyzed data, drafted and edited the manuscript; Barry Honig, Conceptualization, Writing – original draft, Writing – review and editing, Formal analysis, Funding acquisition, Designed experiments, analyzed data, drafted and edited the manuscript

Author ORCIDs

Kerry Marie Goodman  <http://orcid.org/0000-0003-2063-5823>
Phinikoula S Katsamba  <http://orcid.org/0000-0003-3981-1604>

Rotem Rubinstein  <http://orcid.org/0000-0003-3657-5984>

Rosemary V Sampogna  <http://orcid.org/0000-0002-1279-4552>

Lawrence Shapiro  <http://orcid.org/0000-0001-9943-8819>

Barry Honig  <http://orcid.org/0000-0002-2480-6696>

Decision letter and Author response

Decision letter <https://doi.org/10.7554/eLife.72416.sa1>

Author response <https://doi.org/10.7554/eLife.72416.sa2>

Additional files

Supplementary files

- Transparent reporting form

Data availability

Atomic coordinates and structure factors have been deposited in the PDB under the accession codes 7JGZ and 7RGF.

The following datasets were generated:

Author(s)	Year	Dataset title	Dataset URL	Database and Identifier
Goodman KM	2021	Protocadherin gammaC4 EC1-4 crystal structure	https://www.rcsb.org/structure/7JGZ	RCSB Protein Data Bank, 7JGZ
Goodman KM	2021	Protocadherin gammaC4 EC1-4 crystal structure	https://www.rcsb.org/structure/7RGF	RCSB Protein Data Bank, 7RGF

References

- Baldi L**, Hacker DL, Meerschman C, Wurm FM. 2012. Large-Scale Transfection of Mammalian Cells. Hartley JL (Ed). *In Protein Expression in Mammalian Cells: Methods and Protocols*. Totowa, NJ: Humana Press. p. 13–26.
- Barat B**, Wu AM. 2007. Metabolic biotinylation of recombinant antibody by biotin ligase retained in the endoplasmic reticulum. *Biomolecular Engineering* **24**:283–291. DOI: <https://doi.org/10.1016/j.bioeng.2007.02.003>, PMID: 17379573
- Bonn S**, Seeburg PH, Schwarz MK. 2007. Combinatorial expression of alpha- and gamma-protocadherins alters their presenilin-dependent processing. *Molecular and Cellular Biology* **27**:4121–4132. DOI: <https://doi.org/10.1128/MCB.01708-06>, PMID: 17403907
- Brasch J**, Katsamba PS, Harrison OJ, Ahlsén G, Troyanovsky RB, Indra I, Kaczynska A, Kaeser B, Troyanovsky S, Honig B, Shapiro L. 2018. Homophilic and Heterophilic Interactions of Type II Cadherins Identify Specificity Groups Underlying Cell-Adhesive Behavior. *Cell Reports* **23**:1840–1852. DOI: <https://doi.org/10.1016/j.celrep.2018.04.012>, PMID: 29742438
- Brasch J**, Goodman KM, Noble AJ, Rapp M, Mannepalli S, Bahna F, Dandey VP, Bepler T, Berger B, Maniatis T, Potter CS, Carragher B, Honig B, Shapiro L. 2019. Visualization of clustered protocadherin neuronal self-recognition complexes. *Nature* **569**:280–283. DOI: <https://doi.org/10.1038/s41586-019-1089-3>, PMID: 30971825
- Canzio D**, Maniatis T. 2019. The generation of a protocadherin cell-surface recognition code for neural circuit assembly. *Current Opinion in Neurobiology* **59**:213–220. DOI: <https://doi.org/10.1016/j.conb.2019.10.001>, PMID: 31710891
- Chen J**, Lu Y, Meng S, Han MH, Lin C, Wang X. 2009. alpha- and gamma-Protocadherins negatively regulate PYK2. *The Journal of Biological Chemistry* **284**:2880–2890. DOI: <https://doi.org/10.1074/jbc.M807417200>, PMID: 19047047
- Chen WV**, Nwakeze CL, Denny CA, O’Keeffe S, Rieger MA, Mountoufaris G, Kirner A, Dougherty JD, Hen R, Wu Q, Maniatis T. 2017. Pcdhac2 is required for axonal tiling and assembly of serotonergic circuitries in mice. *Science (New York, N.Y.)* **356**:406–411. DOI: <https://doi.org/10.1126/science.aal3231>, PMID: 28450636
- Cooper SR**, Jontes JD, Sotomayor M. 2016. Structural determinants of adhesion by Protocadherin-19 and implications for its role in epilepsy. *eLife* **5**:e18529. DOI: <https://doi.org/10.7554/eLife.18529>, PMID: 27787195
- Cosmanescu F**, Katsamba PS, Sergeeva AP, Ahlsen G, Patel SD, Brewer JJ, Tan L, Xu S, Xiao Q, Nagarkar-Jaiswal S, Nern A, Bellen HJ, Zipursky SL, Honig B, Shapiro L. 2018. Neuron-Subtype-Specific Expression, Interaction Affinities, and Specificity Determinants of DIP/Dpr Cell Recognition Proteins. *Neuron* **100**:1385–1400. DOI: <https://doi.org/10.1016/j.neuron.2018.10.046>, PMID: 30467080
- Crooks GE**, Hon G, Chandonia JM, Brenner SE. 2004. WebLogo: a sequence logo generator. *Genome Research* **14**:1188–1190. DOI: <https://doi.org/10.1101/gr.849004>, PMID: 15173120

- Emsley P**, Lohkamp B, Scott WG, Cowtan K. 2010. Features and development of Coot. *Acta Crystallographica. Section D, Biological Crystallography* **66**:486–501. DOI: <https://doi.org/10.1107/S0907444910007493>, PMID: 20383002
- Esumi S**, Kakazu N, Taguchi Y, Hirayama T, Sasaki A, Hirabayashi T, Koide T, Kitsukawa T, Hamada S, Yagi T. 2005. Monoallelic yet combinatorial expression of variable exons of the protocadherin-alpha gene cluster in single neurons. *Nature Genetics* **37**:171–176. DOI: <https://doi.org/10.1038/ng1500>, PMID: 15640798
- Evans PR**, Murshudov GN. 2013. How good are my data and what is the resolution? *Acta Crystallographica. Section D, Biological Crystallography* **69**:1204–1214. DOI: <https://doi.org/10.1107/S0907444913000061>, PMID: 23793146
- Fan L**, Lu Y, Shen X, Shao H, Suo L, Wu Q. 2018. Alpha protocadherins and Pyk2 kinase regulate cortical neuron migration and cytoskeletal dynamics via Rac1 GTPase and WAVE complex in mice. *eLife* **7**:e35242. DOI: <https://doi.org/10.7554/eLife.35242>, PMID: 29911975
- Fukuda E**, Hamada S, Hasegawa S, Katori S, Sanbo M, Miyakawa T, Yamamoto T, Yamamoto H, Hirabayashi T, Yagi T. 2008. Down-regulation of protocadherin-alpha A isoforms in mice changes contextual fear conditioning and spatial working memory. *The European Journal of Neuroscience* **28**:1362–1376. DOI: <https://doi.org/10.1111/j.1460-9568.2008.06428.x>, PMID: 18973563
- Garrett AM**, Bosch PJ, Steffen DM, Fuller LC, Marcucci CG, Koch AA, Bais P, Weiner JA, Burgess RW. 2019. CRISPR/Cas9 interrogation of the mouse Pcdhg gene cluster reveals a crucial isoform-specific role for Pcdhgc4. *PLoS Genetics* **15**:e1008554. DOI: <https://doi.org/10.1371/journal.pgen.1008554>, PMID: 31877124
- Goodman KM**, Rubinstein R, Thu CA, Manneppalli S, Bahna F, Ahlsén G, Rittenhouse C, Maniatis T, Honig B, Shapiro L. 2016a. γ -Protocadherin structural diversity and functional implications. *eLife* **5**:e20930. DOI: <https://doi.org/10.7554/eLife.20930>, PMID: 27782885
- Goodman KM**, Yamagata M, Jin X, Manneppalli S, Katsamba PS, Ahlsén G, Sergeeva AP, Honig B, Sanes JR, Shapiro L. 2016b. Molecular basis of sidekick-mediated cell-cell adhesion and specificity. *eLife* **5**:e19058. DOI: <https://doi.org/10.7554/eLife.19058>, PMID: 27644106
- Goodman KM**, Rubinstein R, Thu CA, Bahna F, Manneppalli S, Ahlsén G, Rittenhouse C, Maniatis T, Honig B, Shapiro L. 2016c. Structural Basis of Diverse Homophilic Recognition by Clustered α - and β -Protocadherins. *Neuron* **90**:709–723. DOI: <https://doi.org/10.1016/j.neuron.2016.04.004>, PMID: 27161523
- Goodman KM**, Rubinstein R, Dan H, Bahna F, Manneppalli S, Ahlsén G, Aye Thu C, Sampogna RV, Maniatis T, Honig B, Shapiro L. 2017. Protocadherin cis-dimer architecture and recognition unit diversity. *PNAS* **114**:E9829–E9837. DOI: <https://doi.org/10.1073/pnas.1713449114>, PMID: 29087338
- Harrison OJ**, Vendome J, Brasch J, Jin X, Hong S, Katsamba PS, Ahlsen G, Troyanovsky RB, Troyanovsky SM, Honig B, Shapiro L. 2012. Nectin ectodomain structures reveal a canonical adhesive interface. *Nature Structural & Molecular Biology* **19**:906–915. DOI: <https://doi.org/10.1038/nsmb.2366>, PMID: 22902367
- Harrison OJ**, Brasch J, Katsamba PS, Ahlsen G, Noble AJ, Dan H, Sampogna RV, Potter CS, Carragher B, Honig B, Shapiro L. 2020. Family-wide Structural and Biophysical Analysis of Binding Interactions among Non-clustered δ -Protocadherins. *Cell Reports* **30**:2655–2671. DOI: <https://doi.org/10.1016/j.celrep.2020.02.003>, PMID: 32101743
- Hasegawa S**, Kumagai M, Hagihara M, Nishimaru H, Hirano K, Kaneko R, Okayama A, Hirayama T, Sanbo M, Hirabayashi M, Watanabe M, Hirabayashi T, Yagi T. 2016. Distinct and Cooperative Functions for the Protocadherin- α , - β and - γ Clusters in Neuronal Survival and Axon Targeting. *Frontiers in Molecular Neuroscience* **9**:155. DOI: <https://doi.org/10.3389/fnmol.2016.00155>
- Hattori D**, Chen Y, Matthews BJ, Salwinski L, Sabatti C, Grueber WB, Zipursky SL. 2009. Robust discrimination between self and non-self neurites requires thousands of Dscam1 isoforms. *Nature* **461**:644–648. DOI: <https://doi.org/10.1038/nature08431>
- Honig B**, Shapiro L. 2020. Adhesion Protein Structure, Molecular Affinities, and Principles of Cell-Cell Recognition. *Cell* **181**:520–535. DOI: <https://doi.org/10.1016/j.cell.2020.04.010>, PMID: 32359436
- Hudson JD**, Tamilselvan E, Sotomayor M, Cooper SR. 2021. A complete Protocadherin-19 ectodomain model for evaluating epilepsy-causing mutations and potential protein interaction sites. *Structure (London, England)* **29**:1128–1143. DOI: <https://doi.org/10.1016/j.str.2021.07.006>, PMID: 34520737
- Ing-Esteves S**, Kostadinov D, Marocha J, Sing AD, Joseph KS, Laboulaye MA, Sanes JR, Lefebvre JL. 2018. Combinatorial Effects of Alpha- and Gamma-Protocadherins on Neuronal Survival and Dendritic Self-Avoidance. *The Journal of Neuroscience* **38**:2713–2729. DOI: <https://doi.org/10.1523/JNEUROSCI.3035-17.2018>, PMID: 29439167
- Iqbal M**, Maroofian R, Çavdarlı B, Riccardi F, Field M, Banka S, Bubshait DK, Li Y, Hertecant J, Baig SM, Dymont D, Efthymiou S, Abdullah U, Makhdoom EUH, Ali Z, Scherf de Almeida T, Molinari F, Mignon-Ravix C, Chabrol B, Antony J, et al. 2021. Biallelic variants in PCDHGC4 cause a novel neurodevelopmental syndrome with progressive microcephaly, seizures, and joint anomalies. *Genetics in Medicine* **23**:2138–2149. DOI: <https://doi.org/10.1038/s41436-021-01260-4>, PMID: 34244665
- Kabsch W**. 2010. XDS. *Acta Crystallographica. Section D, Biological Crystallography* **66**:125–132. DOI: <https://doi.org/10.1107/S0907444909047337>, PMID: 20124692
- Kaneko R**, Kato H, Kawamura Y, Esumi S, Hirayama T, Hirabayashi T, Yagi T. 2006. Allelic gene regulation of Pcdh-alpha and Pcdh-gamma clusters involving both monoallelic and biallelic expression in single Purkinje cells. *The Journal of Biological Chemistry* **281**:30551–30560. DOI: <https://doi.org/10.1074/jbc.M605677200>, PMID: 16893882

- Katsamba P**, Carroll K, Ahlsen G, Bahna F, Vendome J, Posy S, Rajebhosale M, Price S, Jessell TM, Ben-Shaul A, Shapiro L, Honig BH. 2009. Linking molecular affinity and cellular specificity in cadherin-mediated adhesion. *PNAS* **106**:11594–11599. DOI: <https://doi.org/10.1073/pnas.0905349106>, PMID: 19553217
- Keeler AB**, Schreiner D, Weiner JA. 2015. Protein Kinase C Phosphorylation of a γ -Protocadherin C-terminal Lipid Binding Domain Regulates Focal Adhesion Kinase Inhibition and Dendrite Arborization. *The Journal of Biological Chemistry* **290**:20674–20686. DOI: <https://doi.org/10.1074/jbc.M115.642306>, PMID: 26139604
- Kostadinov D**, Sanes JR. 2015. Protocadherin-dependent dendritic self-avoidance regulates neural connectivity and circuit function. *eLife* **4**:e08964. DOI: <https://doi.org/10.7554/eLife.08964>, PMID: 26140686
- Krissinel E**, Henrick K. 2007. Inference of macromolecular assemblies from crystalline state. *Journal of Molecular Biology* **372**:774–797. DOI: <https://doi.org/10.1016/j.jmb.2007.05.022>, PMID: 17681537
- Lefebvre JL**, Kostadinov D, Chen WV, Maniatis T, Sanes JR. 2012. Protocadherins mediate dendritic self-avoidance in the mammalian nervous system. *Nature* **488**:517–521. DOI: <https://doi.org/10.1038/nature11305>, PMID: 22842903
- Liebschner D**, Afonine PV, Baker ML, Bunkóczi G, Chen VB, Croll TI, Hintze B, Hung LW, Jain S, McCoy AJ, Moriarty NW, Oeffner RD, Poon BK, Prisant MG, Read RJ, Richardson JS, Richardson DC, Sammito MD, Sobolev OV, Stockwell DH, et al. 2019. Macromolecular structure determination using X-rays, neutrons and electrons: recent developments in Phenix. *Acta Crystallographica. Section D, Structural Biology* **75**:861–877. DOI: <https://doi.org/10.1107/S2059798319011471>, PMID: 31588918
- Mah KM**, Houston DW, Weiner JA. 2016. The γ -Protocadherin-C3 isoform inhibits canonical Wnt signalling by binding to and stabilizing Axin1 at the membrane. *Scientific Reports* **6**:31665. DOI: <https://doi.org/10.1038/srep31665>, PMID: 27530555
- Mah KM**, Weiner JA. 2017. Regulation of Wnt signaling by protocadherins. *Seminars in Cell & Developmental Biology* **69**:158–171. DOI: <https://doi.org/10.1016/j.semcdb.2017.07.043>, PMID: 28774578
- McCoy AJ**, Grosse-Kunstleve RW, Adams PD, Winn MD, Storoni LC, Read RJ. 2007. Phaser crystallographic software. *Journal of Applied Crystallography* **40**:658–674. DOI: <https://doi.org/10.1107/S0021889807021206>, PMID: 19461840
- Miura SK**, Martins A, Zhang KX, Graveley BR, Zipursky SL. 2013. Probabilistic splicing of Dscam1 establishes identity at the level of single neurons. *Cell* **155**:1166–1177. DOI: <https://doi.org/10.1016/j.cell.2013.10.018>, PMID: 24267895
- Modak D**, Sotomayor M. 2019. Identification of an adhesive interface for the non-clustered $\delta 1$ protocadherin-1 involved in respiratory diseases. *Communications Biology* **2**:354. DOI: <https://doi.org/10.1038/s42003-019-0586-0>, PMID: 31583286
- Molumby MJ**, Anderson RM, Newbold DJ, Koblesky NK, Garrett AM, Schreiner D, Radley JJ, Weiner JA. 2017. γ -Protocadherins Interact with Neuroligin-1 and Negatively Regulate Dendritic Spine Morphogenesis. *Cell Reports* **18**:2702–2714. DOI: <https://doi.org/10.1016/j.celrep.2017.02.060>, PMID: 28297673
- Mountoufaris G**, Chen WV, Hirabayashi Y, O’Keeffe S, Chevee M, Nwakeze CL, Polleux F, Maniatis T. 2017. Multicenter Pcdh diversity is required for mouse olfactory neural circuit assembly. *Science (New York, N.Y.)* **356**:411–414. DOI: <https://doi.org/10.1126/science.aai8801>, PMID: 28450637
- Mountoufaris G**, Canzio D, Nwakeze CL, Chen WV, Maniatis T. 2018. Writing, Reading, and Translating the Clustered Protocadherin Cell Surface Recognition Code for Neural Circuit Assembly. *Annual Review of Cell and Developmental Biology* **34**:471–493. DOI: <https://doi.org/10.1146/annurev-cellbio-100616-060701>, PMID: 30296392
- Murata Y**, Hamada S, Morishita H, Mutoh T, Yagi T. 2004. Interaction with protocadherin-gamma regulates the cell surface expression of protocadherin-alpha. *The Journal of Biological Chemistry* **279**:49508–49516. DOI: <https://doi.org/10.1074/jbc.M408771200>, PMID: 15347688
- Nicoludis JM**, Lau SY, Schärfe CPI, Marks DS, Weihofen WA, Gaudet R. 2015. Structure and Sequence Analyses of Clustered Protocadherins Reveal Antiparallel Interactions that Mediate Homophilic Specificity. *Structure (London, England)* **23**:2087–2098. DOI: <https://doi.org/10.1016/j.str.2015.09.005>, PMID: 26481813
- Nicoludis JM**, Vogt BE, Green AG, Schärfe CP, Marks DS, Gaudet R. 2016. Antiparallel protocadherin homodimers use distinct affinity- and specificity-mediating regions in cadherin repeats 1–4. *eLife* **5**:e18449. DOI: <https://doi.org/10.7554/eLife.18449>, PMID: 27472898
- Nicoludis JM**, Green AG, Walujkar S, May EJ, Sotomayor M, Marks DS, Gaudet R. 2019. Interaction specificity of clustered protocadherins inferred from sequence covariation and structural analysis. *PNAS* **116**:17825–17830. DOI: <https://doi.org/10.1073/pnas.1821063116>, PMID: 31431536
- Onouchi T**, Kishino-Kaneko Y, Kameshita I, Ishida A, Sueyoshi N. 2015. Regulation of Ca(2+)/calmodulin-dependent protein kinase phosphatase (CaMKP/PPM1F) by protocadherin- γ C5 (Pcdh- γ C5). *Archives of Biochemistry and Biophysics* **585**:109–120. DOI: <https://doi.org/10.1016/j.abb.2015.09.014>, PMID: 26386307
- Pancho A**, Aerts T, Mitsogiannis MD, Seuntjens E. 2020. Protocadherins at the Crossroad of Signaling Pathways. *Frontiers in Molecular Neuroscience* **13**:117. DOI: <https://doi.org/10.3389/fnmol.2020.00117>, PMID: 32694982
- Peek SL**, Mah KM, Weiner JA. 2017. Regulation of neural circuit formation by protocadherins. *Cellular and Molecular Life Sciences* **74**:4133–4157. DOI: <https://doi.org/10.1007/s00018-017-2572-3>, PMID: 28631008
- Petersen TN**, Brunak S, von Heijne G, Nielsen H. 2011. SignalP 4.0: discriminating signal peptides from transmembrane regions. *Nature Methods* **8**:785–786. DOI: <https://doi.org/10.1038/nmeth.1701>, PMID: 21959131
- Pettersen EF**, Goddard TD, Huang CC, Couch GS, Greenblatt DM, Meng EC, Ferrin TE. 2004. UCSF Chimera—a visualization system for exploratory research and analysis. *Journal of Computational Chemistry* **25**:1605–1612. DOI: <https://doi.org/10.1002/jcc.20084>, PMID: 15264254

- Phillips GR**, LaMassa N, Nie YM. 2017. Clustered protocadherin trafficking. *Seminars in Cell & Developmental Biology* **69**:131–139. DOI: <https://doi.org/10.1016/j.semcd.2017.05.001>, PMID: 28478299
- Rich RL**, Myska DG. 2007. Survey of the year 2006 commercial optical biosensor literature. *Journal of Molecular Recognition* **20**:300–366. DOI: <https://doi.org/10.1002/jmr.862>, PMID: 18074396
- Robert X**, Gouet P. 2014. Deciphering key features in protein structures with the new ENDscript server. *Nucleic Acids Research* **42**:W320–W324. DOI: <https://doi.org/10.1093/nar/gku316>, PMID: 24753421
- Rubinstein R**, Thu CA, Goodman KM, Wolcott HN, Bahna F, Manneppalli S, Ahlsen G, Chevee M, Halim A, Clausen H, Maniatis T, Shapiro L, Honig B. 2015. Molecular logic of neuronal self-recognition through protocadherin domain interactions. *Cell* **163**:629–642. DOI: <https://doi.org/10.1016/j.cell.2015.09.026>, PMID: 26478182
- Rubinstein R.**, Goodman KM, Maniatis T, Shapiro L, Honig B. 2017. Structural origins of clustered protocadherin-mediated neuronal barcoding. *Seminars in Cell & Developmental Biology* **69**:140–150. DOI: <https://doi.org/10.1016/j.semcd.2017.07.023>, PMID: 28743640
- Schmucker D**, Clemens JC, Shu H, Worby CA, Xiao J, Muda M, Dixon JE, Zipursky SL. 2000. *Drosophila* Dscam is an axon guidance receptor exhibiting extraordinary molecular diversity. *Cell* **101**:671–684. DOI: [https://doi.org/10.1016/s0092-8674\(00\)80878-8](https://doi.org/10.1016/s0092-8674(00)80878-8), PMID: 10892653
- Schreiner D**, Weiner JA. 2010. Combinatorial homophilic interaction between gamma-protocadherin multimers greatly expands the molecular diversity of cell adhesion. *PNAS* **107**:14893–14898. DOI: <https://doi.org/10.1073/pnas.1004526107>, PMID: 20679223
- Sergeeva AP**, Katsamba PS, Cosmanescu F, Brewer JJ, Ahlsen G, Manneppalli S, Shapiro L, Honig B. 2020. DIP/Dpr interactions and the evolutionary design of specificity in protein families. *Nature Communications* **11**:2125. DOI: <https://doi.org/10.1038/s41467-020-15981-8>, PMID: 32358559
- Shapovalov MV**, Dunbrack RL. 2011. A smoothed backbone-dependent rotamer library for proteins derived from adaptive kernel density estimates and regressions. *Structure (London, England)* **19**:844–858. DOI: <https://doi.org/10.1016/j.str.2011.03.019>, PMID: 21645855
- Sievers F**, Wilm A, Dineen D, Gibson TJ, Karplus K, Li W, Lopez R, McWilliam H, Remmert M, Söding J, Thompson JD, Higgins DG. 2011. Fast, scalable generation of high-quality protein multiple sequence alignments using Clustal Omega. *Molecular Systems Biology* **7**:539. DOI: <https://doi.org/10.1038/msb.2011.75>, PMID: 21988835
- Steffen DM**, Ferri SL, Marcucci CG, Blocklinger KL, Molumby MJ, Abel T, Weiner JA. 2021. The γ -Protocadherins Interact Physically and Functionally with Neuroligin-2 to Negatively Regulate Inhibitory Synapse Density and Are Required for Normal Social Interaction. *Molecular Neurobiology* **58**:2574–2589. DOI: <https://doi.org/10.1007/s12035-020-02263-z>, PMID: 33471287
- Strong M**, Sawaya MR, Wang S, Phillips M, Cascio D, Eisenberg D. 2006. Toward the structural genomics of complexes: crystal structure of a PE/PPE protein complex from *Mycobacterium tuberculosis*. *PNAS* **103**:8060–8065. DOI: <https://doi.org/10.1073/pnas.0602606103>, PMID: 16690741
- Thu CA**, Chen WV, Rubinstein R, Chevee M, Wolcott HN, Felsovalyi KO, Tapia JC, Shapiro L, Honig B, Maniatis T. 2014. Single-cell identity generated by combinatorial homophilic interactions between α , β , and γ protocadherins. *Cell* **158**:1045–1059. DOI: <https://doi.org/10.1016/j.cell.2014.07.012>, PMID: 25171406
- Vendome J**, Felsovalyi K, Song H, Yang Z, Jin X, Brasch J, Harrison OJ, Ahlsen G, Bahna F, Kaczynska A, Katsamba PS, Edmond D, Hubbell WL, Shapiro L, Honig B. 2014. Structural and energetic determinants of adhesive binding specificity in type I cadherins. *PNAS* **111**:E4175–E4184. DOI: <https://doi.org/10.1073/pnas.1416737111>, PMID: 25253890
- Winn MD**, Ballard CC, Cowtan KD, Dodson EJ, Emsley P, Evans PR, Keegan RM, Krissinel EB, Leslie AGW, McCoy A, McNicholas SJ, Murshudov GN, Pannu NS, Potterton EA, Powell HR, Read RJ, Vagin A, Wilson KS. 2011. Overview of the CCP4 suite and current developments. *Acta Crystallographica. Section D, Biological Crystallography* **67**:235–242. DOI: <https://doi.org/10.1107/S0907444910045749>, PMID: 21460441
- Wojtowicz WM**, Flanagan JJ, Millard SS, Zipursky SL, Clemens JC. 2004. Alternative splicing of *Drosophila* Dscam generates axon guidance receptors that exhibit isoform-specific homophilic binding. *Cell* **118**:619–633. DOI: <https://doi.org/10.1016/j.cell.2004.08.021>, PMID: 15339666
- Wojtowicz WM**, Wu W, Andre I, Qian B, Baker D, Zipursky SL. 2007. A vast repertoire of Dscam binding specificities arises from modular interactions of variable Ig domains. *Cell* **130**:1134–1145. DOI: <https://doi.org/10.1016/j.cell.2007.08.026>, PMID: 17889655
- Wu Q**, Maniatis T. 1999. A striking organization of a large family of human neural cadherin-like cell adhesion genes. *Cell* **97**:779–790. DOI: [https://doi.org/10.1016/s0092-8674\(00\)80789-8](https://doi.org/10.1016/s0092-8674(00)80789-8), PMID: 10380929
- Wu Q**, Zhang T, Cheng JF, Kim Y, Grimwood J, Schmutz J, Dickson M, Noonan JP, Zhang MQ, Myers RM, Maniatis T. 2001. Comparative DNA sequence analysis of mouse and human protocadherin gene clusters. *Genome Research* **11**:389–404. DOI: <https://doi.org/10.1101/gr.167301>, PMID: 11230163
- Wu W**, Ahlsen G, Baker D, Shapiro L, Zipursky SL. 2012. Complementary chimeric isoforms reveal Dscam1 binding specificity in vivo. *Neuron* **74**:261–268. DOI: <https://doi.org/10.1016/j.neuron.2012.02.029>, PMID: 22542180
- Wu Y**, Honig B, Ben-Shaul A. 2013. Theory and simulations of adhesion receptor dimerization on membrane surfaces. *Biophysical Journal* **104**:1221–1229. DOI: <https://doi.org/10.1016/j.bpj.2013.02.009>, PMID: 23528081
- Zipursky SL**, Grueber WB. 2013. The Molecular Basis of Self-Avoidance. *Annual Review of Neuroscience* **36**:547–568. DOI: <https://doi.org/10.1146/annurev-neuro-062111-150414>

Appendix 1

Appendix 1—key resources table

Reagent type (species) or resource	Designation	Source or reference	Identifiers	Additional information
Strain, strain background (<i>E. coli</i>)	One shot Top10 Competent Cells	Invitrogen	C4040-06	Plasmid production
Cell line (<i>Homo sapiens</i>)	FreeStyle 293 F cells	Thermo Fisher Scientific	R79007	Cell line for protein expression
Cell line (<i>Homo sapiens</i>)	K-562 bone marrow chronic myelogenous leukemia (CML) cells	ATCC	ATCC CCL-243	Cell line for cell-aggregation assays
Transfected construct (<i>M. musculus</i>)	$\alpha_{4_{1-5}}$	This paper		Pcdh α 4 EC1–5, Honig/Shapiro labs
Transfected construct (<i>M. musculus</i>)	$\alpha_{7_{1-5}}$	Rubinstein et al., 2015		
Transfected construct (<i>M. musculus</i>)	$\alpha_{12_{1-5}}$	This paper		Pcdh α 12 EC1–5, Honig/Shapiro labs
Transfected construct (<i>M. musculus</i>)	$\beta_{6_{1-4}}$	Goodman et al., 2016c		
Transfected construct (<i>M. musculus</i>)	$\beta_{8_{1-4}}$	Goodman et al., 2016c		
Transfected construct (<i>M. musculus</i>)	$\gamma_{A1_{1-4}}$	Goodman et al., 2016a		
Transfected construct (<i>M. musculus</i>)	$\gamma_{A4_{1-4}}$	Goodman et al., 2016a		
Transfected construct (<i>M. musculus</i>)	$\gamma_{A8_{1-4}}$	Rubinstein et al., 2015		
Transfected construct (<i>M. musculus</i>)	$\gamma_{A9_{1-5}}$	Goodman et al., 2016a		
Transfected construct (<i>M. musculus</i>)	$\gamma_{B2_{1-5}}$	Goodman et al., 2016a		
Transfected construct (<i>M. musculus</i>)	$\gamma_{B4_{1-5}}$	This paper		Pcdh γ B4 EC1–5, Honig/Shapiro labs
Transfected construct (<i>M. musculus</i>)	$\gamma_{B5_{1-4}}$	Goodman et al., 2016a		
Transfected construct (<i>M. musculus</i>)	$\alpha_{C2_{1-4}}$	Rubinstein et al., 2015		
Transfected construct (<i>M. musculus</i>)	$\gamma_{C3_{1-4}}$	Goodman et al., 2016a		
Transfected construct (<i>M. musculus</i>)	$\gamma_{C4_{1-4}}$	This paper		Pcdh γ C4 EC1–4, Honig/Shapiro labs

Appendix 1 Continued on next page

Appendix 1 Continued

Reagent type (species) or resource	Designation	Source or reference	Identifiers	Additional information
Transfected construct (<i>M. musculus</i>)	γ C5 ₁₋₅	Rubinstein et al., 2015		
Transfected construct (<i>M. musculus</i>)	α 7 ₁₋₅ -AVI	This paper		Biotinylated Pcdh α 7 EC1–5, Honig/Shapiro labs
Transfected construct (<i>M. musculus</i>)	β 6 ₁₋₄ -AVI	This paper		Biotinylated Pcdh β 6 EC1–4, Honig/Shapiro labs
Transfected construct (<i>M. musculus</i>)	β 8 ₁₋₄ -AVI	This paper		Biotinylated Pcdh β 8 EC1–4, Honig/Shapiro labs
Transfected construct (<i>M. musculus</i>)	γ A8 ₁₋₄ -AVI	This paper		Biotinylated Pcdh γ A8 EC1–4, Honig/Shapiro labs
Transfected construct (<i>M. musculus</i>)	γ A9 ₁₋₅ -AVI	This paper		Biotinylated Pcdh γ A9 EC1–5, Honig/Shapiro labs
Transfected construct (<i>M. musculus</i>)	γ B2 ₁₋₅ -AVI	This paper		Biotinylated Pcdh γ B2 EC1–5, Honig/Shapiro labs
Transfected construct (<i>M. musculus</i>)	α C2 ₁₋₄ -AVI	This paper		Biotinylated Pcdh α C2 EC1–4, Honig/Shapiro labs
Transfected construct (<i>M. musculus</i>)	γ C3 ₁₋₄ -AVI	This paper		Biotinylated Pcdh γ C3 EC1–4, Honig/Shapiro labs
Transfected construct (<i>M. musculus</i>)	γ C4 ₁₋₄ -AVI	This paper		Biotinylated Pcdh γ C4 EC1–4, Honig/Shapiro labs
Transfected construct (<i>M. musculus</i>)	γ C5 ₁₋₅ -AVI	This paper		Biotinylated Pcdh γ C5 EC1–5, Honig/Shapiro labs
Transfected construct (<i>M. musculus</i>)	α 4 ₁₋₄ -AVI	This paper		Biotinylated Pcdh α 4 EC1–4, Honig/Shapiro labs
Transfected construct (<i>M. musculus</i>)	α 7 ₁₋₅ L301R	This paper		Pcdh α 7 EC1–5 mutant, Honig/Shapiro labs
Transfected construct (<i>M. musculus</i>)	γ A8 ₁₋₄ I116R	Rubinstein et al., 2015		Pcdh γ A8 EC1–4 mutant, Honig/Shapiro labs
Transfected construct (<i>M. musculus</i>)	β 6 ₁₋₄ R41N	This paper		Pcdh β 6 EC1–4 mutant, Honig/Shapiro labs
Transfected construct (<i>M. musculus</i>)	γ C5 ₁₋₅ S116R	This paper		Pcdh γ C5 EC1–5 mutant, Honig/Shapiro labs
Transfected construct (<i>M. musculus</i>)	β 6 ₁₋₄ S117I	This paper		Pcdh β 6 EC1–4 mutant, Honig/Shapiro labs
Transfected construct (<i>M. musculus</i>)	β 6 ₁₋₄ L125P	This paper		Pcdh β 6 EC1–4 mutant, Honig/Shapiro labs
Transfected construct (<i>M. musculus</i>)	β 6 ₁₋₄ E369K	This paper		Pcdh β 6 EC1–4 mutant, Honig/Shapiro labs

Appendix 1 Continued on next page

Appendix 1 Continued

Reagent type (species) or resource	Designation	Source or reference	Identifiers	Additional information
Transfected construct (<i>M. musculus</i>)	$\beta_{6_{1-4}}$ Y371F	This paper		Pcdh β_6 EC1–4 mutant, Honig/Shapiro labs
Transfected construct (<i>M. musculus</i>)	$\beta_{6_{1-4}}$ R41N/S117I	This paper		Pcdh β_6 EC1–4 mutant, Honig/Shapiro labs
Transfected construct (<i>M. musculus</i>)	$\beta_{6_{1-4}}$ R41N/E369K	This paper		Pcdh β_6 EC1–4 mutant, Honig/Shapiro labs
Transfected construct (<i>M. musculus</i>)	$\beta_{6_{1-4}}$ S117I/L125P	This paper		Pcdh β_6 EC1–4 mutant, Honig/Shapiro labs
Transfected construct (<i>M. musculus</i>)	$\beta_{6_{1-4}}$ R41N/S117I/L125P	This paper		Pcdh β_6 EC1–4 mutant, Honig/Shapiro labs
Transfected construct (<i>M. musculus</i>)	$\beta_{6_{1-4}}$ R41N/S117I/E369K	This paper		Pcdh β_6 EC1–4 mutant, Honig/Shapiro labs
Transfected construct (<i>M. musculus</i>)	$\beta_{6_{1-4}}$ R41N/S117I/Y371F	This paper		Pcdh β_6 EC1–4 mutant, Honig/Shapiro labs
Transfected construct (<i>M. musculus</i>)	$\beta_{6_{1-4}}$ R41N/S117I/L125P/E369K/Y371F	This paper		Pcdh β_6 EC1–4 mutant, Honig/Shapiro labs
Transfected construct (<i>M. musculus</i>)	$\gamma_{C4_{1-4}}$ E78A	This paper		PcdhyC4 EC1–4 mutant, Honig/Shapiro labs
Transfected construct (<i>M. musculus</i>)	$\gamma_{C4_{1-4}}$ E78Q	This paper		PcdhyC4 EC1–4 mutant, Honig/Shapiro labs
Transfected construct (<i>M. musculus</i>)	$\gamma_{C4_{1-4}}$ S344R	This paper		PcdhyC4 EC1–4 mutant, Honig/Shapiro labs
Transfected construct (<i>M. musculus</i>)	$\gamma_{C4_{1-4}}$ D290A	This paper		PcdhyC4 EC1–4 mutant, Honig/Shapiro labs
Transfected construct (<i>M. musculus</i>)	$\gamma_{C4_{1-4}}$ D290N	This paper		PcdhyC4 EC1–4 mutant, Honig/Shapiro labs
Transfected construct (<i>M. musculus</i>)	$\beta_{1_{3-6}}$	This paper		Pcdh β_1 EC3–6, Honig/Shapiro labs
Transfected construct (<i>M. musculus</i>)	$\beta_{6_{1-6}}$	This paper		Pcdh β_6 EC1–6, Honig/Shapiro labs
Transfected construct (<i>M. musculus</i>)	$\beta_{9_{3-6}}$	This paper		Pcdh β_9 EC3–6, Honig/Shapiro labs
Transfected construct (<i>M. musculus</i>)	$\gamma_{A3_{3-6}}$	This paper		PcdhyA3 EC3–6, Honig/Shapiro labs
Transfected construct (<i>M. musculus</i>)	$\gamma_{A4_{3-6}}$	Goodman et al., 2016a		
Transfected construct (<i>M. musculus</i>)	$\gamma_{A9_{3-6}}$	This paper		PcdhyA9 EC3–6, Honig/Shapiro labs

Appendix 1 Continued on next page

Appendix 1 Continued

Reagent type (species) or resource	Designation	Source or reference	Identifiers	Additional information
Transfected construct (<i>M. musculus</i>)	γ B2 ₃₋₆	Goodman et al., 2016a		
Transfected construct (<i>M. musculus</i>)	γ B5 ₃₋₆	Goodman et al., 2016a		
Transfected construct (<i>M. musculus</i>)	γ B7 ₃₋₆	Goodman et al., 2016a		
Transfected construct (<i>M. musculus</i>)	α C2 ₂₋₆	Goodman et al., 2016a		
Transfected construct (<i>M. musculus</i>)	α 7 ₁₋₅ / γ C3 ₆ chimera	Goodman et al., 2016a		
Transfected construct (<i>M. musculus</i>)	γ C3 ₃₋₆	Goodman et al., 2016a		
Transfected construct (<i>M. musculus</i>)	γ C5 ₂₋₆	This paper		PcdhyC5 EC2–6, Honig/Shapiro labs
Transfected construct (<i>M. musculus</i>)	β 9 ₃₋₆ -AVI	This paper		Biotinylated Pcdh β 9 EC3–6, Honig/Shapiro labs
Transfected construct (<i>M. musculus</i>)	γ A4 ₃₋₆ -AVI	This paper		Biotinylated PcdhyA4 EC3–6, Honig/Shapiro labs
Transfected construct (<i>M. musculus</i>)	γ A9 ₃₋₆ -AVI	This paper		Biotinylated PcdhyA9 EC3–6, Honig/Shapiro labs
Transfected construct (<i>M. musculus</i>)	γ B2 ₃₋₆ -AVI	This paper		Biotinylated PcdhyB2 EC3–6, Honig/Shapiro labs
Transfected construct (<i>M. musculus</i>)	α C2 ₃₋₆ -AVI	This paper		Biotinylated Pcdh α C2 EC3–6, Honig/Shapiro labs
Transfected construct (<i>M. musculus</i>)	γ C3 ₃₋₆ -AVI	This paper		Biotinylated PcdhyC3 EC3–6, Honig/Shapiro labs
Transfected construct (<i>M. musculus</i>)	γ C5 ₂₋₆ -AVI	This paper		Biotinylated PcdhyC5 EC2–6, Honig/Shapiro labs
Transfected construct (<i>M. musculus</i>)	γ A4 ₃₋₆ V560R	This paper		PcdhyA4 EC3–6 mutant, Honig/Shapiro labs
Transfected construct (<i>M. musculus</i>)	γ C3 ₃₋₆ V560R	This paper		PcdhyC3 EC3–6 mutant, Honig/Shapiro labs
Transfected construct (<i>M. musculus</i>)	γ A4 ₃₋₆ K558R	This paper		PcdhyA4 EC3–6 mutant, Honig/Shapiro labs
Transfected construct (<i>M. musculus</i>)	γ C3 ₃₋₆ R558K	This paper		PcdhyC3 EC3–6 mutant, Honig/Shapiro labs
Transfected construct (<i>M. musculus</i>)	γ B7 ₃₋₆ Y532G	Goodman et al., 2017		

Appendix 1 Continued on next page

Appendix 1 Continued

Reagent type (species) or resource	Designation	Source or reference	Identifiers	Additional information
Transfected construct (<i>M. musculus</i>)	γ B7 ₃₋₆ A570R	This paper		PcdhyB7 EC3-6 mutant, Honig/Shapiro labs
Peptide, recombinant protein	NeutrAvidin-HRP	Thermo Fisher Scientific	31,030	Biotinylated protein western bot
Peptide, recombinant protein	NeutrAvidin protein	Thermo Fisher Scientific	31,000	SPR assays
Peptide, recombinant protein	BSA	Sigma-Aldrich	A7906	SPR assays
Commercial assay or kit	Spin Miniprep Kit	Qiagen	27,106	
Commercial assay or kit	Hi-speed Plasmid Maxi Kit	Qiagen	12,663	
Commercial assay or kit	SF Cell Line 4D-Nucleofector X Kit S	Lonza	V4XC-2032	
Commercial assay or kit	Amine-coupling kit	Cytiva	BR100050	SPR experiments
Commercial assay or kit	Morpheus Amino Acids	Molecular Dimensions	MD2-100-77	Crystallography
Commercial assay or kit	Morpheus Buffer System II	Molecular Dimensions	MD2-100-101	Crystallography
Chemical compound	Polyethylenimine	Polysciences	24765-2	Transfection
Chemical compound	Biotin	Sigma-Aldrich	B4501	Protein biotinylation
Chemical compound	Tris Base	Fisher Scientific	BP152-5	
Chemical compound	Sodium Chloride	Fisher Scientific	S271-10	
Chemical compound	Calcium Chloride Dihydrate	JT Baker	1336-01	
Chemical compound	Imidazole	ACROS	301870025	
Chemical compound	HEPES	Sigma-Aldrich	H3375	
Chemical compound	Tween-20	Sigma-Aldrich	P7949	
Chemical compound	Sodium Acetate	Sigma-Aldrich	S7545	
Chemical compound	IMAC Sepharose 6 Fast Flow	Cytiva	17092109	
Chemical compound	Penicillin Streptomycin	Thermo Fisher Scientific	15070063	
Chemical compound	PEG 6000	Sigma-Aldrich	81,260	
Chemical compound	PEG 8000	Sigma-Aldrich	89,510	
Chemical compound	Ethylene Glycol	Fluka	03760	
Chemical compound	Lithium Chloride	Sigma-Aldrich	L8895	
Chemical compound	MES	Sigma-Aldrich	M3671	
Chemical compound	Glycerol	ACROS	332031000	
Software, algorithm	UCLA Diffraction Anisotropy Server	Strong et al., 2006		https://srv.mbi.ucla.edu/Anisoscalf/
Software, algorithm	SednTerp	Thomas Laue		http://bitwiki.sr.unh.edu/index.php/Main_Page
Software, algorithm	HeteroAnalysis			https://core.uconn.edu/auf
Software, algorithm	Scrubber 2.0	BioLogic Software		http://www.biologic.com.au

Appendix 1 Continued on next page

Appendix 1 Continued

Reagent type (species) or resource	Designation	Source or reference	Identifiers	Additional information
Software, algorithm	Phaser	McCoy et al., 2007		Implemented in CCP4 or Phenix (see below)
Software, algorithm	CCP4	Winn et al., 2011		https://www.ccp4.ac.uk/
Software, algorithm	Phenix	Liebschner et al., 2019		http://www.hkl-xray.com/
Software, algorithm	XDS	Kabsch, 2010		http://xds.mpimf-heidelberg.mpg.de
Software, algorithm	AIMLESS	Evans and Murshudov, 2013		http://www.ccp4.ac.uk
Software, algorithm	Coot	Emsley et al., 2010		https://www2.mrc-lmb.cam.ac.uk/personal/pemsley/coot/
Software, algorithm	PISA	Krissinel and Henrick, 2007		http://www.ebi.ac.uk/pdbe/protint/pistart.html
Software, algorithm	Pymol	Schrödinger		https://pymol.org
Software, algorithm	UCSF Chimera	Pettersen et al., 2004		https://www.cgl.ucsf.edu/chimera/
Software, algorithm	Clustal Omega	Sievers et al., 2011		https://www.ebi.ac.uk/Tools/msa/clustalo/
Software, algorithm	WebLogo 3.0	Crooks et al., 2004		http://weblogo.threeplusone.com/
Software, algorithm	SignalP 4.0	Petersen et al., 2011		https://services.healthtech.dtu.dk/service.php?SignalP-5.0
Software, algorithm	ASTRA	Wyatt		https://www.wyatt.com/products/software/astra.html
Other	Freestyle 23 Expression Media	Thermo Fisher Scientific	12338-018	Protein expression media
Other	Opti-MEM Reduced Serum Media	Thermo Fisher Scientific	31985-070	Protein expression media
Other	Series S CM4 chip	Cytiva	BR100539	SPR assays
Other	Fetal Bovine Serum	Thermo Fisher Scientific	16141079	Cell-aggregation assays media
Other	DMEM with GlutaMAX	Thermo Fisher Scientific	10569010	Cell-aggregation assays media